Vegetation-modulated landscape evolution: Effects of vegetation on landscape processes, drainage density, and topography

Erkan Istanbulluoglu and Rafael L. Bras

Department of Civil and Environmental Engineering, Massachusetts Institute of Technology, Cambridge, Massachusetts, USA

Received 8 October 2004; revised 13 February 2005; accepted 28 February 2005; published 8 June 2005.

[1] Topography acts as a template for numerous landscape processes that include hydrologic, ecologic, and biologic phenomena. These processes not only interact with each other but also contribute to shaping the landscape as they influence geomorphic processes. We have investigated the effects of vegetation on thresholds for channel initiation and landform evolution using both analytical and numerical approaches. Vegetation is assumed to form a uniform ground cover. Runoff erosion is modeled based on a power function of excess shear stress, in which shear stress efficiency is inversely proportional to vegetation cover. This approach is validated using data. Plant effect on slope stability is represented by additional cohesion provided by plant roots. Vegetation cover is assumed to reduce sediment transport rates due to physical creep processes (rainsplash, dry ravel, and expansion and contraction of sediments) according to a negative exponential relationship. Vegetation grows as a function of both available cover and unoccupied space by plants and is killed by geomorphic disturbances (runoff erosion and landsliding) and wildfires. Analytical results suggest that in an equilibrium basin with a fixed vegetation cover, plants may cause a transition in the dominant erosion process at the channel head. A runoff erosion–dominated landscape, under none or poor vegetation cover, may become landslide dominated under a denser vegetation cover. The sign of the predicted relationship between drainage density and vegetation cover depends on the relative influence of vegetation on different erosion phenomena. With model parameter values representative of the Oregon Coast Range (OCR), numerical experiments conducted using the Channel Hillslope Integrated Landscape Development (CHILD) model confirm the findings based on the analytical theory. A highly dissected fluvial landscape emerges when surface is assumed bare. When vegetation cover is modeled, landscape relief increases, resulting in hollow erosion dominated by landsliding. Interestingly, our simulations underscore the importance of vegetation disturbances by geomorphic events and wildfires on the landscape structure. Simulated landscapes resemble real-world catchments in the OCR when such disturbances are considered.

Citation: Istanbulluoglu, E., and R. L. Bras (2005), Vegetation-modulated landscape evolution: Effects of vegetation on landscape processes, drainage density, and topography, *J. Geophys. Res.*, *110*, F02012, doi:10.1029/2004JF000249.

1. Introduction

[2] Hydrologic, ecologic and geomorphic processes in a river basin are inherently coupled. On the one hand, natural vegetation patterns result from the interplay between climate, soils and topography; on the other, vegetation in turn exerts important controls on the hydrologic and geomorphic processes in the basin, and contributes to the formation of landscape morphology over the long term.

[3] Vegetation is clearly an important factor in geomorphology. Pioneering studies were mostly qualitative and described potential effects of vegetation on the surface processes [e.g., *Cotton*, 1955]. Arguably, the first detailed study that relates hydrology, geomorphology and vegetation at a watershed scale, was Hack and Goodlet's survey of the upper Shenandoah Valley, Virginia [*Hack and Goodlett*, 1960]. Their work revealed important correlations between topographic form and forest type. More recent work sought relationships between landscape topography and vegetation patterns in a wider range of ecology, climate and landscape conditions [e.g., *Florinsky and Kuryakova*, 1996; *Pickup and Chewings*, 1996].

[4] By enhancing the soil strength for runoff erosion and landsliding, vegetation cover may impose an upper limit to the extent of the drainage network [e.g., *Horton*, 1945; *Prosser*, 1996; *Prosser and Soufi*, 1998], a plausible reason why the data of *Melton* [1957] shows an inverse relationship between drainage density, a length scale that shows the degree of dissection of the landscape, and humidity. Similarly to Melton's work, *Gregory and Gardiner* [1975] and *Gregory* [1976] presented data showing large variability

0148-0227/05/2004JF000249$09.00

in drainage density under a dry climate regime and much smaller variability as climate becomes more humid. A number of studies also proposed a complex relationship between climate and sediment yields, modulated by vegetation [*Langbein and Schumm*, 1958; *Wilson*, 1973]. These studies showed both drainage density and sediment yields increasing with precipitation in arid and semiarid areas, reaching a peak in an intermediate precipitation regime and reducing as climate becomes wetter. Both the drainage density and sediment yields are limited by a lack of erosive storms under weak climate forcing. As runoff erosion increases with mean annual precipitation, so do drainage density and sediment yields, until the wetter climate supports the growth of vegetation capable of limiting erosion in an increasingly erosive environment [*Moglen et al.*, 1998].

[5] Although the above references mostly attributed the observed changes in the data to trends in the climate and vegetation, spatial variations in soil and rock erodibility [*Moglen and Bras*, 1995; *Howard*, 1994], variations in the climate forcing [*Tucker and Bras*, 2000], and tectonic activity [*Whipple*, 2001; *Tucker and Whipple*, 2002; *Tucker*, 2004] can influence both sediment yields and drainage density. The time frame over which these observations are valid is also unclear. Given that long-term erosion rates tend to balance the mass supplied by tectonic uplift, a period of reduced erosion due to resistant vegetation would likely be counterbalanced with times of increased erosion activity. A good example of this is self-driven cycles of hollow infilling and evacuation, typically observed in vegetated humid environments [*Dietrich et al.*, 1986; *Benda and Dunne*, 1997; *Kirchner et al.*, 2001], where the level of vegetation resistance was argued to control both the frequency and magnitude of sediment yields [*Istanbulluoglu et al.*, 2004].

[6] Some recent landscape models incorporate the effects of vegetation on erosion, with interest in different timescales. Such models use simple noncompetitive vegetation dynamics independent of soil moisture and basin shape. These studies include modeling soil erosion over short timescales (years to decades) in cultivated lands [*Foster*, 1982; *Arnold et al.*, 1995; *Mitas and Mitasova*, 1998]; centurial- to millennial-scale interactions between erosion and vegetation [*Benda and Dunne*, 1997; *Lancaster et al.*, 2003; *Gabet and Dunne*, 2003b; *Istanbulluoglu et al.*, 2004]; and the development of fluvial topography over geomorphic timescales [*Collins et al.*, 2004]. Consistent with some field evidence, modeling suggested a reduction in drainage density, and increased episodicity in sediment fluxes owing to resistant vegetation cover [*Collins et al.*, 2004; *Istanbulluoglu et al.*, 2004].

[7] Interactions between vegetation, hydrology and landscape development is inherently complex. It is conceivable that plant response to soil moisture deficit [*Porporato et al.*, 2001], plant suitability to climate and soil conditions [*Laio et al.*, 2001; *Porporato et al.*, 2003], and coexistence of different species and functional types [*van Wijk and Rodriguez-Iturbe*, 2002; *Fernandez-Illescas and Rodriquez-Iturbe*, 2004] would have important implications for erosion rates and resulting landscape morphology. However, using a simple vegetation growth function seems to be a relevant preliminary strategy, although it will be applicable only in regions where plant growth is not limited by water. With this in mind, a number of fundamental questions in the interface between ecology and geomorphology remain to be explored. These include issues such as: What is the level of vegetation influence on sediment yields, and resulting valley formation and drainage density over short and long timescales? What are the large-scale implications of the coupling between vegetation and erosion dynamics and tectonic uplift? Are there any morphologic landscape properties that could be diagnostic of former vegetation patterns on the landscape? Are there any characteristic response timescales of landscapes to changes in external forcing with and without vegetation cover? Can one identify relevant plant physiological characteristics whose role should be further investigated in the field?

[8] Of particular interest in this paper is to investigate the effects of vegetation on landscape development. To do so, first we present theory that relates water erosion, hillslope diffusion and landsliding to vegetation cover. The concept of shear stress partitioning, pioneered by *Einstein and Barbarossa* [1952] and followed by others [*Foster*, 1982; *Rauws*, 1988], is utilized to model the effects of vegetation cover on flow shear stress and resulting erosion and landscape development. Data reported from flume experiments conducted by *Prosser et al.* [1995] on a vegetated hillslope is used to calibrate the shear stress partitioning model. Hillslope diffusivity is assumed to decrease with increasing vegetation cover according to an exponential function, in agreement with some field evidence and an earlier model [*Malmon and Dunne*, 1996; *Alberts et al.*, 1995]. Threshold slope gradient for landslide initiation is related to vegetation cover through root cohesion. Second, we derive expressions for channel initiation by overland flow and landsliding for hillslopes in equilibrium. We then investigate the sensitivity of channel head source area and drainage density to steady state erosion, runoff rate and vegetation cover. This analysis reveals a transition in the dominant erosion process at the channel head mediated by vegetation cover. Thirdly, numerical simulations are performed using the Channel Hillslope Integrated Landscape Development (CHILD) model [*Tucker et al.*, 2001b, 2001c] to investigate the effects of dynamic vegetation cover on the large-scale landscape evolution.

2. Model Formulation

[9] The model presented below provides the basis for the channel head source area functions derived in section 4. The theory is also implemented to the CHILD landscape evolution model to explore the implications of vegetation on landscape evolution.

2.1. Water Erosion and Sediment Transport: Effects of Vegetation on Flow Shear Stress

[10] The local rate of stream incision is commonly represented by two types of erosion models: detachment limited and transport limited erosion. The detachment limited erosion model typically ignores the effects of upslope sediment supply on the rate of local lowering, and predicts erosion as a function of local flow erosivity [*Howard*, 1980, 1994, 1997]. In the transport limited model, the local rate of erosion or deposition depends on the difference between the capacity of water in transporting sediment and the rate of sediment influx [*Kirkby*, 1971;

Willgoose et al., 1991]. In streams where sufficient, easily detachable sediment is always available for transport, the latter model predicts local erosion as the divergence of sediment transport capacity. Some so-called hybrid models attempt to account for both local detachment capacity and potential effects of lateral sediment flux on river incision rates [*Tucker and Whipple*, 2002; *Whipple and Tucker*, 2002]. In bedrock channels, sediment flux may play an important role in river incision by providing the tools for abrasion and plugging and sometimes protecting the bed from saltating particles, yielding complex model formulations [*Sklar and Dietrich*, 1998, 2004]. Appropriate for alluvial rivers and soil mantled hillslopes are models that either limit erosion rate to the lesser of detachment or the excess sediment transport capacity [*Tucker and Slingerland*, 1997; *Tucker et al.*, 2001b],

$$\frac{\partial z}{\partial t} = -\mathrm{Min}[D_c, \nabla q_s], \tag{1}$$

or relate erosion linearly to the fraction of excess stream carrying capacity [*Foster*, 1982; *Foster et al.*, 1995],

$$\frac{\partial z}{\partial t} = -D_c\left(1 - \frac{q_s}{q_{tc}}\right), \tag{2}$$

where D_c is detachment capacity (L/T), q_s is sediment load, and q_{Tc} is sediment transport capacity of the unit flow width (L^2/T).

[11] Both detachment and sediment transport capacity can be postulated as a power function of excess shear stress [*Yang*, 1996; *Nearing et al.*, 1999]; for detachment capacity this can be written as

$$D_c = k_e(\tau_b - \tau_c)^p \tag{3}$$

$$\tau_b = \rho_w g R S, \tag{4}$$

where k_e is soil erodibility, τ_b is the boundary shear stress, τ_c is the critical shear stress for sediment entrainment, ρ_w, is the water density, g is gravity of acceleration, R is hydraulic radius, and S is local slope. Exponent p is usually between 1.5 and 3 for stream sediment transport capacity [*Yang*, 1996; *Engelund and Hansen*, 1967], and erosion of soil mantled hillslopes [*Nearing et al.*, 1999], but usually lower for bedrock erosion [*Howard and Kerby*, 1983].

[12] Some complex models relate various vegetation properties to flow conditions in channels to represent the hydrodynamic effects of vegetation on the flow, such as transport and turbulence processes around plants [i.e., *Freeman et al.*, 2000; *Nepf*, 1999; *Nepf and Vivoni*, 2000]. Here in the interest of developing a parsimonious model that can be calibrated and used for long-term landscape evolution simulations, we use a much simpler, yet physically plausible approach to model potential effects of vegetation on overland flow depths and erosion rates.

[13] Considering the relative contributions of sediment and channel form on flow roughness, *Einstein and Barbarossa* [1952] proposed to partition the boundary shear stress into grain and form roughness components:

$$\tau_b = \tau_g + \tau_{fo} = \rho_w g R_g S + \rho_w g R_{fo} S, \tag{5}$$

where τ_g and τ_{fo} are grain and form shear stress, and R_g and R_{fo} are effective hydraulic radii due to grain and form resistance components, respectively. In this model, grain shear stress is responsible for sediment transport. This theory is supported by data from rivers and overland flow field experiments [*Yang*, 1996; *Govers and Rauws*, 1986; *Rauws*, 1988, *Nearing et al.*, 1997].

[14] Following the same logic, *Foster* [1982] proposed to relate the shear stress available for soil erosion in crop lands to the boundary shear stress using a shear stress partitioning fraction as

$$\tau_f = \tau_b \frac{f_s}{f_t}, \tag{6}$$

where τ_f is effective shear stress acting on the soil surface, and f_s and f_t are Darcy-Weisbach friction factors for bare soil and total roughness for the composite surface. The factor f_t includes resistance due to crop residue, surface litter, and bare soil. In the equation, f_s/f_t is known as the shear stress partitioning ratio. Note that in this model *Foster* [1982] proposed to use the soil friction factor instead of grain friction, primarily because grain roughness is often difficult to distinguish from form roughness on hillslopes due to microtopography of the soil surface. *Prosser et al.* [1995] applied this model to their experimental data where they obtained f_s and f_t from observed flow depth and velocity in the flume under different vegetation cover conditions. The Darcy-Weisbach friction factor is traditionally estimated by plotting f against Reynolds number, Re, $f \propto Re^{\psi}$ as in the Moody diagram, where $Re = uy/\nu$; u is flow velocity, y is flow depth and ν is kinematic viscosity of the flow. In theory, both the sign and the magnitude of ψ change as a function of flow regime, with significant deviations on naturally vegetated surfaces [*Prosser and Slade*, 1994; *Prosser et al.*, 1995; *Prosser and Dietrich*, 1995; *Abrahams et al.*, 1995]. *Abrahams and Parsons* [1994] found that variations in f as a function of Re are considerably less than variations due to changes in the form resistance itself (due to microtopography, stone cover, and vegetation), and that f can be treated independent of Re for purposes of overland flow modeling [*Howes and Abrahams*, 2003]. This is in agreement with other field studies that estimated f from hydrograph analysis of experimental field plots [*Foster et al.*, 1968; *Engman*, 1986], and with numerical models [*Woolhiser et al.*, 1990; *Gilley and Weltz*, 1995].

[15] An alternative approach to using the Darcy-Weisbach friction factor is to use the Manning's equation in calculating the effective shear stress. Total Manning's roughness coefficient, n_t, and hydraulic radius, R_t, can be partitioned into bare soil and vegetation components, represented by subscripts of s and V, as

$$n_t = n_s + n_V \tag{7a}$$

$$R_t = R_s + R_V. \tag{7b}$$

Other additional roughness factors such as obstructions to the flow in channels can be added to (7a) and (7b) as appropriate. After partitioning hydraulic radius this way, effective shear stress and resulting erosion can be written as

a function of R_s [*Einstein and Barbarossa*, 1952]. Following *Laursen* [1958], we can express R_s as functions of the average flow velocity of the compound vegetation-bare soil cover:

$$R_s = \left(n_s \frac{u}{S^{1/2}} \right)^{3/2}, \tag{8}$$

where u is average overland flow velocity. Substituting Manning's equation, $u = (n_s + n_V)^{-1} R_t^{2/3} S^{1/2}$, into (8), hydraulic radius for bare soil becomes a function of the total hydraulic radius, R_t:

$$R_s = R_t \left[\frac{n_s}{n_s + n_V} \right]^{3/2}. \tag{9}$$

Next, writing R_t in terms of discharge and local slope, $R_t = (n_s + n_v)^m q^m S^{n-1}$ [e.g., *Willgoose et al.*, 1991; *Istanbulluoglu et al.*, 2003], and substituting into equation (4), the effective shear stress, acting on the soil surface, τ_f, can be expressed as

$$\tau_f = \tau_b F_\tau = \beta q^m S^n F_\tau \tag{10}$$

$$F_\tau = \left(\frac{n_s}{n_s + n_V} \right)^{3/2}, \tag{11}$$

where F_τ is the shear stress partitioning ratio written as a function of Manning's roughness coefficient for bare soil and vegetation, q is unit discharge, S is slope, and β, m and n are parameters that may vary with flow geometry. For overland flow and flow in large rectangular channels, $m = 6/10$, $n = 7/10$, $q = Q/W$ and $\beta = \rho_w g (n_s + n_V)^{6/10}$, where Q is total discharge and W is flow width.

[16] In the equations above, effective shear stress is partly a function of vegetation roughness. We now need to relate vegetation roughness to vegetation cover in order to relate dynamic changes in the vegetation cover to flow hydraulics, as has been qualitatively suggested in a number of experimental works [e.g., *Ree et al.*, 1977; *Engman*, 1986]. We assume that roughness due to a particular vegetation can be parameterized as a power function of its ground cover fraction relative to a reference vegetation, V_R, which has a known roughness coefficient, n_{vR} according to [*Istanbulluoglu et al.*, 2004]

$$n_V = n_{VR} \left(\frac{V}{V_R} \right)^{\omega}. \tag{12}$$

On the basis of this assumption, hydraulic radius, R_t, equivalent to flow depth for overland flow, and effective shear stress, τ_f, are written as functions of vegetation cover fraction respectively as

$$R_t = \left(n_s + n_{VR} \left[\frac{V}{V_R} \right]^{\omega} \right)^{6/10} q^{6/10} S^{-3/10} \tag{13}$$

$$\tau_f = \frac{\rho_w g n_s^{1.5}}{\left(n_s + n_{VR} \left[\frac{V}{V_R} \right]^{\omega} \right)^{9/10}} q^{6/10} S^{7/10}. \tag{14}$$

In equations (12), (13), and (14), the parameter ω quantifies the dependence of vegetation roughness to surface vegetation cover. In section 3, we use field observations reported by *Prosser et al.* [1995] to estimate this parameter for grass.

2.2. Hillslope Diffusion

[17] The rate of change in the landscape elevation caused by slope-dependent diffusive processes is given by

$$\frac{\partial z}{\partial t} = -\nabla q_{sd}. \tag{15}$$

In gentle slopes, sediment transport by hillslope diffusion is often parameterized as a linear function of slope gradient, S, $q_s = K_d S$ [*McKean et al.*, 1993]. More recent field evidence suggests that as slopes approach a threshold limit for sliding, sediment flux increases infinitely [*Roering et al.*, 1999, 2001]. Both linear and nonlinear dependence of hillslope diffusion to slope gradient can be represented by [*Howard*, 1994, 1997; *Roering et al.*, 1999, 2001]

$$q_{sd} = \frac{K_d S}{1 - (S/S_c)^2}, \tag{16}$$

where K_d is a diffusion constant (L^2/T), and S_c is the critical gradient for sliding of dry soil.

[18] On bare soils, hillslope diffusivity is predominantly controlled by rainsplash, expansion and contraction of sediments due to freeze-thaw, wet-dry cycles and dry ravel [e.g., *Gabet*, 2003]. Some field observations show up to an order of magnitude higher soil creep rates in bare and loosely vegetated soils compared to vegetated slopes [*Young*, 1972; *Selby*, 1974; *Carson and Kirkby*, 1972; *Jahn*, 1981, 1989]. Over a period of more than twenty years, *Jahn* [1981, 1989] measured soil creep rates in three ecological zones in the Sudetes Mountains of Poland. Soil creep under grass was several times higher than under pasture cover. For over twelve years no creep was observed beneath a mature forest even on slopes as steep as 30°. These differences were attributed to the binding effects of vegetation roots [*Selby*, 1993].

[19] In contrast, other studies report significantly higher soil creep rates in forested humid basins dominated by bioturbation, which accounts for disturbances due to tree throw, root growth and decay in the soil profile and burrowing animals [*Roering et al.*, 2002; *Black and Montgomery*, 1991; *Nash*, 1980] compared to creep rates in less vegetated and arid environments [*Hanks*, 2000]. Recent data from the Oregon Coast Range indicate that on average approximately 4 m^3 soil is displaced by each tree throw event, which plausibly produce transport rate constants on average >0.01 m^2/yr. Therefore it is arguable that the works cited in the previous paragraph, suggesting lower creep rates in forested slopes, did not capture any tree throw events in forests [*Jahn*, 1981, 1989].

[20] In the literature presented above there is little or no information on the relative contributions of different creep processes to the hillslope diffusivity constant, nor on the quantitative relations of diffusivity to climate, soil type and vegetation cover. In the Water Erosion Prediction Project (WEPP) model [*Alberts et al.*, 1995] the erodibility parameter for slope-dependent interill erosion for rangelands

decreases exponentially with vegetation cover, as plant cover shields the surface from freeze-thaw, wet-dry cycles and rainsplash. *Malmon and Dunne* [1996] studied the role of different factors on sediment transport driven by rainsplash under simulated rainfall. Among other factors, they found that sediment transport rate due to rainsplash shows a negative exponential dependence on vegetation cover, in agreement with some other data [*Selby*, 1974; *Jahn*, 1981, 1989; *Moss*, 1989]. Following the studies cited above, we relate diffusion constant to surface vegetation cover according to an exponential function

$$K_d = K_b\left[e^{-\alpha V}\right], \tag{17}$$

where K_b is a baseline diffusion constant (L^2/T), and α is an empirical parameter. The term in brackets may be thought of as an adjustment factor that accounts for the influence of vegetation on physical soil creep processes, including rainsplash, freeze-thaw, and dry ravel. In the WEPP model $\alpha = -7.0$ for rangelands. For rainsplash, *Malmon and Dunne* [1996] gave this parameter as a function of median rain drop size, D, (cm) in the form, $\alpha = -0.718D^{-1.28}$. The baseline diffusivity constant represents aggregate effects of all other creep processes [*Roering et al.*, 1999, 2002]. By implicitly representing the effects of vegetation on sediment transport due to rainsplash, freeze-tow, and wet-dry cycles, the model presented above can be potentially used for investigating the impacts of temporary vegetation loss on sediment yields, such as forest clearing, wildfires and vegetation change [*Wells*, 1987; *Davis et al.*, 1989], and the implications of physical creep processes on long-term landscape evolution. The limitation of this model is that it does not account for the contribution of bioturbation disturbances (e.g., growth and death of trees, tree throw, animal burrowing), and vegetation is only assumed to reduce transport rates by protecting the surface from rainsplash, freeze-tow and wet-dry cycles.

2.3. Landslide Initiation

[21] In the infinite slope stability equation root strength contributes to the stabilizing factors by adding apparent cohesion to the soil [*Wu and Sidle*, 1995; *Benda and Dunne*, 1997; *Lancaster et al.*, 2003]:

$$FS = \frac{C_r + C_s}{h_s\rho_s g\sin\theta} + \frac{\cos\theta\tan\phi[1 - R_w\rho_w/\rho_s]}{\sin\theta}, \tag{18}$$

where FS is the ratio of resisting to driving forces, C_r and C_s are root and soil cohesion respectively, h_s is soil thickness perpendicular to slope, θ and ϕ are ground slope and soil internal friction angles, R_w is the relative wetness, defined as the ratio of subsurface flow depth flowing parallel to the soil surface to soil thickness and ρ_s is soil density. Under steady state subsurface flow, R_w can be expressed as the ratio of steady state lateral subsurface flow discharge, PA, to the lateral flux capacity, TS [*Montgomery and Dietrich*, 1994]:

$$R_w = \begin{cases} \dfrac{PA}{TS}, & \dfrac{A}{S} < \dfrac{T}{P} \\ 1, & \dfrac{A}{S} \geq \dfrac{T}{P} \end{cases}, \tag{19}$$

where T is lateral soil transmissivity (L^2/T), and P is steady state water input rate (L/T). The relative wetness has an upper bound of unity, with full saturation of the soil profile. In this model ground saturation occurs when $A/S \geq T/P$, where T/P can be thought of as a topographic threshold for saturation.

[22] Equation (18) can be written in the form of a critical slope threshold that depends on drainage area, by equating $FS = 1$, and solving for slope. For cohesionless soils, by relating root cohesion to surface vegetation cover, and expressing root cohesion and relative wetness in normalized forms, we can write

$$S_c = \frac{C_r' V}{\cos\theta} + \tan\phi\left[1 - \rho_w/\rho_s \min\left(\Gamma\frac{A}{S}, 1\right)\right], \tag{20}$$

where, C_r' is mature root cohesion for complete vegetation cover normalized to soil weight, $C_r' = C_r/h_s\rho_s g$, and Γ is a hydrology parameter that is the ratio of steady state precipitation rate to soil transmissivity, $\Gamma = P/T$, or the inverse of the saturation threshold. This normalization reduces the number of variables related to soils and vegetation in which there is significant uncertainty [*Nielson et al.*, 1973; *Moore et al.*, 1986]. In this equation, by multiplying C_r' with V, we assume that total root cohesion in a hillslope parcel is linearly proportional to surface vegetation cover. Root reinforcement may vary among different plant species and functional types, and depending on the root depth, however, for the purposes of modeling vegetation effects on landform development over geological timescales, relating total cohesion linearly with vegetation cover seems to be a rational assumption which also has some field justification [*Abe and Ziemer*, 1991; *Schmidt et al.*, 2001; *Roering et al.*, 2003].

3. Influence of Surface Vegetation on Overland Flow Hydraulics: Data Analysis

[23] We used published data to test the hypothesized relationship between Manning's roughness and vegetation cover (equation (12)), and its applicability in an excess shear stress erosion model. *Prosser et al.* [1995] conducted field experiments using a 6 m long, 0.3 m wide and 0.3 m high flume to investigate the effects of vegetation cover on overland flow sediment yields in two field plots in the Tennessee Valley area of Marin County, California. The experimental plots were located along the axis of a grass covered hollow on a 15° slope, with initial ground cover fractions of 95% and 75%. The plot with denser vegetation cover was typical of the prevailing vegetation conditions in the area, while the other was chosen because of its lower vegetation density and rougher surface [*Prosser et al.*, 1995].

[24] Four experiments were carried out over the first plot: undisturbed (95% vegetation cover), first clipped (50–55%), second clipped (35–40%) and fully clipped (10%) conditions. Two experiments were run over the second plot, for undisturbed (75%) and fully clipped (10%) conditions. *Prosser et al.* [1995] reported steady state flow discharge, average values of the flow depths and total soil loss volume measured in each experimental run. To depict the influence of vegetation on overland flow erosion, first we plot soil loss observed in each experiment against the boundary shear

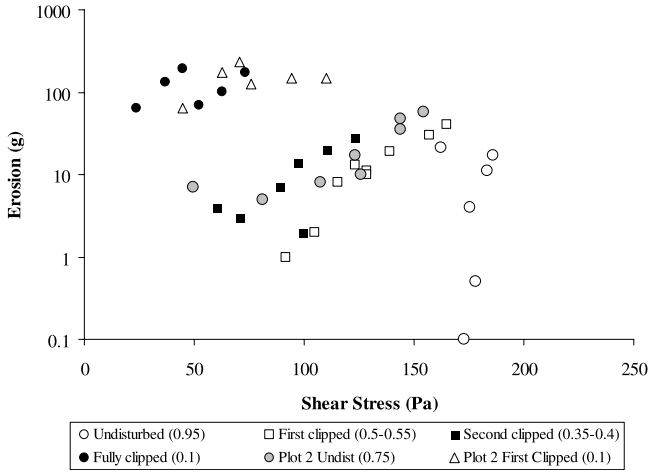

Figure 1. Soil loss as a function of total shear stress. Data are from *Prosser et al.* [1995].

stress, calculated using the reported flow depths and valley slope. In Figure 1, the relationship between erosion and boundary shear stress cannot be represented by a single power function in the form of equation (3), as was earlier reported for bare soil field plots [*Moore et al.*, 1986; *Laflen et al.*, 1991; *Nearing et al.*, 1997, 1999]. Although applied shear stresses are high in their experiment, soil loss under vegetation cover is limited to trivial amounts [*Prosser et al.*, 1995]. For a given boundary shear stress, reduction or cessation in the soil loss under a denser cover suggests that effective shear stress is inversely related to vegetation cover. This qualitatively supports the effective shear stress formulation presented in equation (14).

[25] The next step in relating vegetation cover to shear stress is to estimate an appropriate value for the exponent ω in (12). Vegetation cover and water discharge data reported for each run, and slope of the field flume, are used in equation (13) to estimate a value for ω that minimizes the differences between the measured and calculated flow depths. To do this analysis we need to select values for Manning's roughness for bare soil and mature vegetation cover (equation (13)). For dense grass surfaces, *Engman* [1986] reported total Manning's roughness coefficients obtained from field experiments, including the roughness of both soil and vegetation, $n_s + n_{VR}$, up to 0.65 for natural rangelands. Following *Engman* [1986], we set the total surface roughness for mature grass cover, $n_s + n_{VR}$ to 0.65. The reference vegetation cover V_R is assumed to be 95%, as reported by *Prosser et al.* [1995] for their undisturbed plots. Manning's roughness for bare soil is assumed to be 0.025 for the first plot. In order to represent relatively rougher surface conditions in the second, we used a higher soil roughness value of 0.035. These values are within the range of values recommended for overland flow in naturally eroded soils [*Engman*, 1986; *Woolhiser et al.*, 1990; *American Society of Civil Engineers*, 1996].

[26] Figure 2 plots the observed flow depths against the calculated using equation (13). The best fit between the observed and calculated flow depths is obtained with ω = 0.5. It is conceivable that this exponent would vary depending on the vegetation characteristics. The correlation between the observed and calculated flow depths gives an R^2 of 0.81, with a regression slope of 1. Without the simple relationship used in equation (12), a roughness value for each vegetation cover has to be specified to calculate flow velocity.

[27] Next, we plot, in Figure 3, effective shear stress (equation (14)) minus a threshold shear stress against the reported soil loss. The erosion threshold is assumed to be 0.6 Pa, the value calculated from the vegetation and flow data reported for the experiment with no soil loss [*Prosser et al.*, 1995]. Although there is significant scatter in the graph, sediment yields under different vegetation cover tend to collapse toward a single line. In Figure 3, the straight lines are solutions of equation (3) fitted to the data using $p = 2$ with three different erodibility values. Results presented here support the findings of *Prosser et al.* [1995] that resistance due to vegetation can be additive to bed resistance in reducing the flow velocity, and that on vegetated surfaces a greater fraction of the shear stress is exerted on vegetation than on soils, reducing the detachment potential

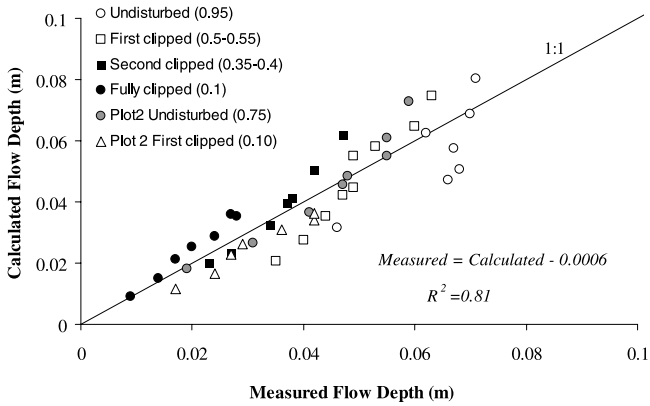

Figure 2. Measured versus calculated average flow depths for ω = 0.5. In the legend, numbers in parentheses are ground cover fractions reported for each run by *Prosser et al.* [1995]. In the calculations the midvalue is used whenever vegetation cover is reported as a range.

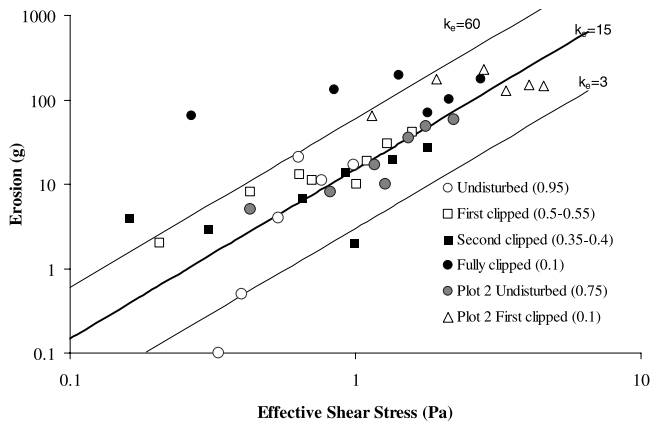

Figure 3. Soil loss as a function of effective shear stress. Lines plot equation (3) using $p = 2$ and erodibility values of 3, 15, and 60 that encompass a large fraction of the observed soil loss.

of water. The simple function that relates vegetation roughness to vegetation cover (equation (12)) provides a way to relate erosion potential to vegetation cover.

4. Control of Vegetation in the Channel Head Source Area: Analytical Results

[28] The theory described above can be used to investigate the effects of vegetation on the landscape structure. The degree of landscape dissection, often known as drainage density, is among the most fundamental properties of the landscape. Drainage density is strongly correlated with the valley or channel head source area: that is the basin size where the transition from convex or straight hillslopes to concave valleys, or to well-defined channels occurs [*Montgomery and Dietrich*, 1989; *Moglen et al.*, 1998]. The hillslope-valley transition represents a shift in process dominance, where soil removal by area- and slope-dependent erosion processes such as runoff erosion and pore pressure driven landsliding outpace slope-dependent diffusive sediment transport that tends to fill channels with hillslope colluvium [*Smith and Bretherton*, 1972; *Willgoose et al.*, 1991; *Tarboton et al.*, 1992; *Howard*, 1997; *Moglen et al.*, 1998]. In humid landscapes, where vegetation actively restrains sheetwash, channels may begin with an abrupt channel head where a landscape threshold is exceeded. Channel initiation by saturation overland flow [*Kirkby and Chorley*, 1967; *Dietrich et al.*, 1993; *Istanbulluoglu et al.*, 2002], seepage erosion [*Dunne*, 1990] and landsliding [*Montgomery and Dietrich*, 1988, 1994] are among these thresholds.

[29] To identify the potential environmental factors controlling the location of the channel head, we obtained source area expressions for channel initiation by overland flow and landsliding for equilibrium landscapes, where erosion rate is in balance with uplift. Above the channel head, sediment transport is assumed to be controlled by diffusive hillslope processes. For the sake of simplicity, and consistent with the threshold channel initiation hypothesis [*Montgomery and Dietrich*, 1994; *Prosser and Dietrich*, 1995], we assume that in vegetated hillslopes, once an erosion threshold is exceeded, erosion potential in the channel is always so high that channel infilling by diffusive sediment transport from the sides of the channel head is negligible. In keeping the analyses simple we neglect the effects of stochastic precipitation [*Tucker and Bras*, 2000; *Benda and Dunne*, 1997], and heterogeneity in vegetation and soils. Such heterogeneities and process uncertainties often result in spatial variations in the topographic thresholds for channel initiation [*Montgomery and Dietrich*, 1994; *Istanbulluoglu et al.*, 2002], and resulting drainage density [*Tucker et al.*, 2001a]. Consequently, given these simplifications, the expressions presented below should only be considered simple approximations that provide some indication of the dependence of source area to uplift rate, vegetation cover, and runoff.

[30] For analytical tractability we assume that hillslope sediment transport is linearly proportional to hillslope gradient. Steady state water discharge is calculated as a function of unit contributing area and a geomorphically effective runoff, P_e:

$$q = P_e A. \tag{21}$$

[31] In a steady state basin, where erosion is in balance with tectonic uplift or base level drop, the relationship between hillslope gradient and contributing area can be obtained by equating sediment production to hillslope sediment transport:

$$UA = K_d S, \tag{22}$$

where U is the steady state erosion rate that is equal to tectonic uplift over the long term, and A is unit contributing area. Substituting equation (17) for K_d to represent the effects of vegetation on soil creep and solving for slope gives the equilibrium hillslope gradient as

$$S_{eq} = U_* e^{\alpha V} A, \tag{23}$$

where U_* is the ratio of steady state erosion rate to bare soil diffusivity, $U_* = U/K_b$ here referred to as hillslope steepness index. This is analogous to the channel steepness index, which is often used to describe the power law dependence of local channel slope with basin area [*Whipple*, 2001; *Kobor and Roering*, 2004].

[32] The source area for runoff erosion is the point at which the hillslope gradient becomes steep enough so that overland flow shear stress is greater than or just equal to the erosion threshold. This can be defined by substituting equation (21) and equation (23) into equation (14), setting equation (14) equal to the erosion threshold, τ_c, and finally solving for A to obtain

$$A_R = \left[\frac{\tau_c \left(n_s + n_{VR} \left(\frac{V}{V_R} \right)^{\omega} \right)^{9/10}}{\rho_w g n_s^{1.5} P_e^{6/10} \left(U_* e^{\alpha V} \right)^{7/10}} \right]^{\frac{1}{0.6+0.7}}, \tag{24}$$

where, A_R is the source area for runoff erosion.

[33] In many steep, soil mantled landscapes, channels often begin with a shallow debris flow scar [*Montgomery and Dietrich*, 1988]. Here we derive landsliding source area relationships both for bare and vegetated hillslopes. In the absence of vegetation and soil cohesion, slope stability is a function of the angle of repose of the hillslope material and subsurface flow pore pressure. Thus neglecting the first term in equation (20) ($C_r' = 0$ and $V = 0$), substituting the equilibrium hillslope gradient for hillslope sediment transport into the slope term in the subsurface flow transport model in (20), and solving for area gives the basin size for threshold landsliding. Here, the threshold for ground saturation plays an important role in the source area size. In the steady state subsurface flow model, described in equations (19) and (20), ground saturation occurs when $A/S \geq \Gamma^{-1}$. Solving for S gives the maximum slope required for saturation, S_s, for a given unit contributing area as, $S_s = \Gamma A$, and saturation occurs when $S \leq S_s(A)$. Note that both the equilibrium slope gradient S_{eq} (equation (23)) and threshold slope for saturation are linearly proportional to A, suggesting that when $U_* > \Gamma$, the equilibrium hillslope gradient, for a given A, is always greater than the slope required for ground saturation. Thus with this condition, valley formation by threshold landsliding begins in unsat-

urated portions of the landscape with a source area expressed by

$$A_L = U_*^{-1} \tan\phi \left[1 - \frac{\rho_w}{\rho_s} \Gamma U_*^{-1}\right] \qquad U_* > \Gamma, \tag{25}$$

where, A_L is the area at which equilibrium hillslope gradient becomes just steep enough for the initiation of pore pressure activated landsliding. When $\Gamma \geq U_*$ equilibrium hillslope gradient is always smaller than the slope required for ground saturation, leading to valley formation by saturated landsliding when local area is larger than

$$A_L = U_*^{-1} \tan\phi \left[1 - \frac{\rho_w}{\rho_s}\right] \qquad \Gamma \geq U_*. \tag{26}$$

[34] For the case when vegetation interacts with both physical soil creep processes and landslide initiation, remembering that $\cos\theta = 1/\sqrt{S+1}$ in equation (20) and substituting equation (23) into the slope terms in the right hand side of equation (20) gives a quadratic function in the form

$$\mathrm{X} A_L^2 + \mathbf{Y} A_L + \mathrm{Z} = 0, \tag{27}$$

where

$$\mathrm{X} = \left(1 - \left(C_r' V\right)^2\right)\left(U_* e^{\alpha V}\right)^2, \tag{28a}$$

$$\mathbf{Y} = -2\Lambda U_* e^{\alpha V}, \tag{28b}$$

$$\mathrm{Z} = \Lambda^2 - \left(C_r' V\right)^2, \tag{28c}$$

$$\Lambda = \tan\phi \left[1 - \frac{\rho_w}{\rho_s} \min\left(\Gamma\left(U_* e^{\alpha V}\right)^{-1}, 1\right)\right]. \tag{28d}$$

Note that when $V = 0$, Λ gives the threshold slope gradient for landsliding for nonvegetated hillslopes, and that equation (27) reduces to equation (25) or (26) depending on U_* and Γ.

[35] Sensitivity analysis of the equations described above is one way to investigate the effects of vegetation, climate and other environmental factors on channel head source area. Of particular interest here is the influence of vegetation on the landscape structure. Two of these effects we discuss here are (1) vegetation control on the source area and drainage density when the valley head position is strictly maintained by either of the two erosion mechanisms, runoff erosion or landsliding, and (2) vegetation as a mediator of the dominant erosion process at the channel head.

[36] Figure 4a plots source area for overland flow as a function of slope steepness factor U_*, runoff rate P_e, and vegetation cover V. In the plot, U_*, P_e and V are normalized to arbitrarily selected reference values that produce an input range between 0.01 and 10 for each parameter. Source area is normalized to the threshold basin size calculated using the selected reference values of all three parameters. In

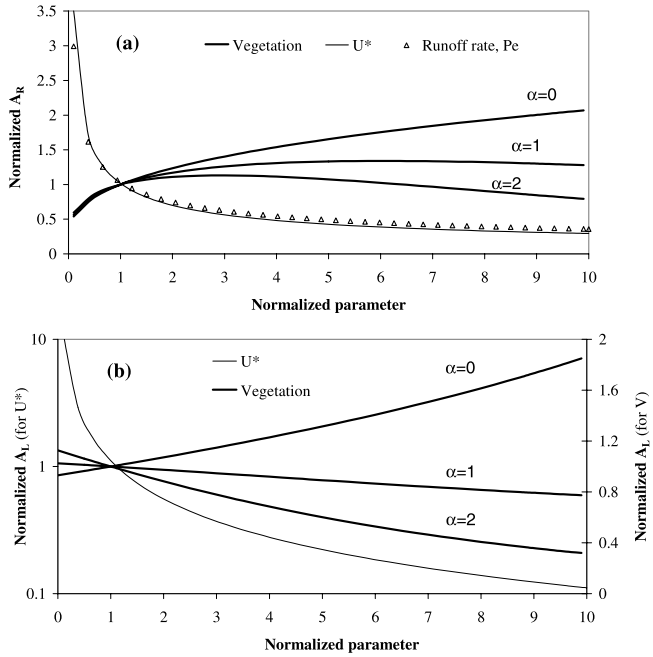

Figure 4. Sensitivity of channel head source area to slope steepness factor U_*, runoff rate P_e, and vegetation cover V for channel initiation due to (a) runoff and (b) landsliding. In the plots, effects of vegetation on hillslope diffusivity are represented by different values of α.

examining the sensitivity of source area to vegetation cover, dependence of soil diffusivity on vegetation is represented by different values of α.

[37] While there is a power law relationship between runoff erosion source area and U_* and P_e, such that $A_R \propto U_*^{-0.56} P_e^{-0.46}$, source area exhibits a more complex response to changes in the vegetation cover. When vegetation does not influence diffusion rates, and for relatively small values of soil roughness, source area scales with vegetation cover according to a power function, $A_R \propto V^{0.34}$. This dependence directly reflects the effects of vegetation cover on reducing the shear stress efficiency, which consequently increases the size of the zero-order basin. For $\alpha > 0$, the proportionality between threshold source area and vegetation cover can be written as, $A_R \propto V^{0.34} e^{-\alpha 0.54 V}$. The second term in this relationship accounts for the effects of vegetation in reducing the soil creep rates (i.e., by surface shielding, binding effects of roots). Vegetation-induced reduction in soil creep causes a more rapid slope steepening with area to maintain a constant rate of erosion in equilibrium with uplift. Because overland flow shear stress is more sensitive to slope, $\tau \propto A^{0.6} S^{0.7}$, for a given vegetation cover, an increase in the equilibrium slope at the channel head results in a reduction in the basin size for channel initiation. This interplay between the contrasting effects of vegetation on flow hydraulics and soil diffusion could produce, depending on α, a maximum for channel head source area, where A_R first increases as a function of V, then decreases after reaching a peak. On the left side of the maximum source area, effects of vegetation on flow hydraulics dominate, such that a denser vegetation cover requires a larger source area to incise a channel. However

on the right, effects of vegetation on soil creep dominates, steepening the local slopes and resulting in a reduction in the source area size. This behavior can be observed in the relationship between A_R and V plotted using $\alpha = 2$ (Figure 4a).

[38] In the absence of vegetation cover, source basin size for threshold landsliding, A_L scales negatively with the hillslope steepness index, U_*, $A_L \propto U_*^{-1}$, where the exponent is unity for both saturated, and dry failures (Figure 4b), but slightly smaller in the case of unsaturated landslides (not plotted). We found, by regressing vegetation cover with source area that, when vegetation does not influence hillslope diffusion ($\alpha = 0$), source area for landsliding is related to vegetation cover exponentially, in the form: $A_L \propto e^{\varepsilon V}$, where ε is a scaling factor that depends on additional cohesion by vegetation roots in the model. For typical conditions in the forested western United States, with root cohesion of 10 to 14 kPa, one meter effective root depth, and Γ in the range of 0.001–0.002 [*Dietrich et al.*, 1993; *Istanbulluoglu et al.*, 2002], ε is 0.1 ± 0.05.

[39] As in the case of runoff erosion, under a fixed vegetation cover, a stronger influence of vegetation on reducing the hillslope diffusion rates (i.e., higher α), yields a smaller source area for landsliding. A reduction in the soil creep rates with vegetation cover creates steeper equilibrium hillslope gradients. On steeper ground, the triggering of landslides requires a smaller pore pressure forcing that results in the reduction of the threshold basin size. In the model, landsliding source area is positively related to vegetation cover when, per increase in the vegetation cover, increase in the threshold slope for landsliding (equation (21)) is higher than the vegetation-modulated increase in the equilibrium slope gradient. This requires a larger source area for slopes to be just as steep as the critical slope for landsliding.

[40] Source area has an important implication on the structure of drainage basins. On the basis of DEM data analysis of seven basins in the United States, *Moglen et al.* [1998] found that drainage density consistently exhibits a power law relationship with source area:

$$D_d \propto A_s^{-\Theta}, \tag{29}$$

where Θ narrowly varies between 0.45 and 0.57. For the purposes of argument here, we assume $\Theta = 0.5$, and substitute the channel head source area relationships derived for threshold-dominated conditions. For overland flow, drainage density is positively related to the hillslope steepness index, U_* (meaning positively to U, negatively to K_b) and runoff, P_e, and negatively related to vegetation cover according to $D_{dR} \propto U_*^{0.28}.P_e^{0.23}\ V^{-0.15}$. For landsliding, $D_{dL} \propto U_*^{0.47}\ e^{-0.05V}$. Note that in these proportionalities, vegetation influence on diffusion rates is neglected ($\alpha = 0$). The analysis suggests a higher sensitivity in the drainage density of landslide-dominated valleys to tectonic uplift, and hillslope diffusion, than in their low-relief fluvial counterparts where channels are maintained by the exceedence of runoff erosion thresholds. In contrast, channel head locations in fluvial systems seem to be more sensitive to vegetation cover.

[41] In discussing the implications of different environmental controls on the dominant processes that control drainage density, it is useful first to identify which of the two processes described above controls the drainage density in an equilibrium basin. Here we define the landscape source area as the smaller of the source areas defined separately for runoff erosion and landsliding:

$$A_s = \min[A_R, A_L]. \tag{30}$$

This description allows for a transition in the active erosion process at the channel head in response to changes in the forcing and vegetation cover.

[42] We plot source area for runoff erosion and landsliding, both normalized to the mean of the latter, and drainage density, normalized to its mean value, as functions of vegetation cover under a high, moderate and low values of hillslope steepness index, U_*, which are $U_* = 0.1$, $U_* = 0.01$ and $U_* = 0.001$ respectively (Figure 5). For comparison, these steepness indexes correspond to mean erosion rates U, of 1 mm/yr, 0.1 mm/yr and 0.01 mm/yr respectively for a fixed hillslope diffusivity constant of $K_b = 0.01$ m^2/yr. When the hillslope steepness index is high (first column in Figure 5), corresponding to $U \sim 1$ mm/yr, zero-order basin size is dictated by landsliding in the analytical model. This is because in the example, for all values of α, the source area for channel initiation by landsliding is always lower than the source area for runoff erosion. With no influence on the physical creep rates, vegetation causes up to twofold decrease in the drainage density (first figure). In contrast, as α increases, drainage density also increases with vegetation because of slope steepening as a response to slower creep transport under vegetation cover. In the other extreme case, characterized by low U_*, the source area for fluvial channel incision is always smaller than the threshold drainage area for shallow landsliding, as is typical of low-relief regions, resulting in "erosion-dominated" valleys [*Tucker and Bras*, 1998]. As in the landsliding case, vegetation, if does not affect diffusion rates, results in smaller drainage density, as source area is positively related to vegetation cover. However, depending on the degree of vegetation effect on reducing the slope-dependent physical creep rates, in our model, drainage density may first decrease with vegetation cover and then increase.

[43] Perhaps the most interesting example here is the intermediate case, in which the variation in the vegetation cover not only alters the size of the zero-order basin controlled by one process, but also produces a shift in the dominant erosion process controlling the valley head position (equation (30)). In all three cases with progressively increasing α (top to bottom in the second column in Figure 5), runoff erosion is responsible for channel initiation when vegetation is sparse. Process transition at the channel head occurs, when the source area for fluvial erosion, augmented by increasing vegetation cover, becomes larger than that of landsliding, at which point the dominant process switches to landsliding. While such a shift occurs with 10% vegetation cover in the example, this number varies depending on the values of other model parameters. Here we have provided this analysis as a proof-of-concept of the potential implications of vegetation on processes dominance and landscape dissection. A thorough sensitivity analysis of the model to investigate the conditions that lead to a transition in the dominant erosion processes at the channel head is still needed.

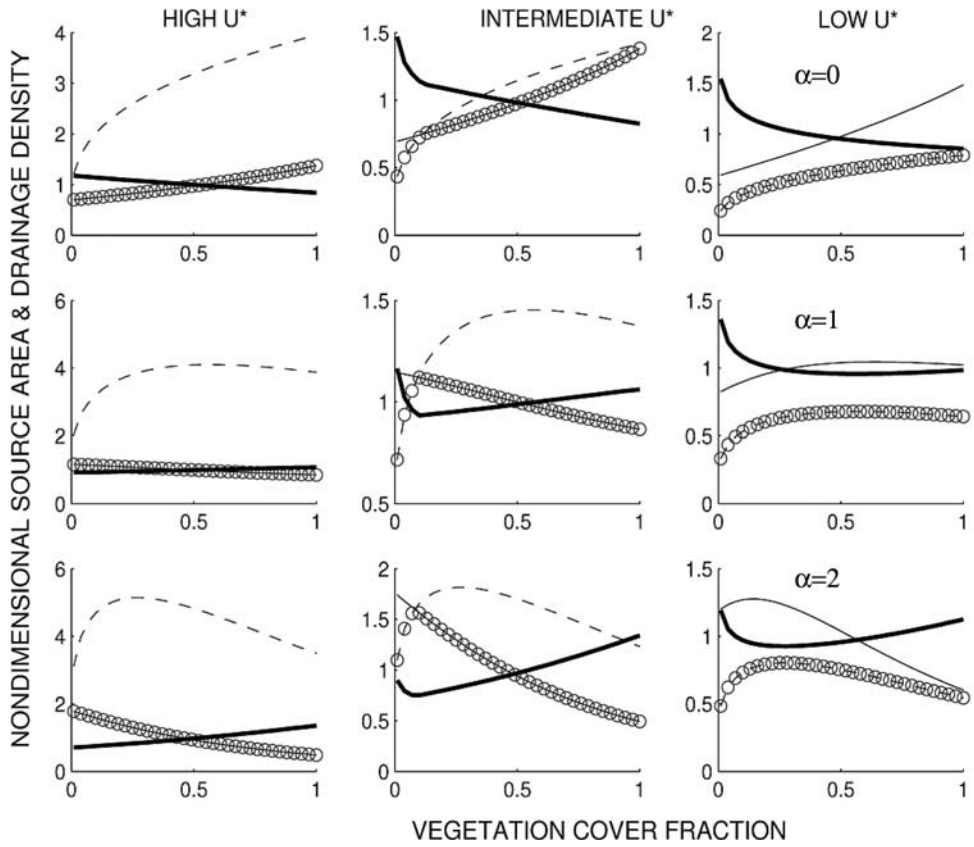

Figure 5. Nondimensional source area and drainage density as a function of vegetation cover for high, intermediate, and low values of the hillslope steepnes factor U_* for (top) $\alpha = 0$, (middle) $\alpha = 1$, and (bottom) $\alpha = 2$. Plots show runoff source area (dashed line), landsliding source area (solid line), landscape source area (circles), and the drainage density (bold line). Model parameters used in this example are $P_e = 5$ mm/h, $K_b = 0.01$ m^2/yr, $\tau_c = 1$ Pa, $n_b = 0.03$, $n_V = 0.3$, $\Gamma = 0.01$, $\phi = 35°$, and $C_r' = 0.4$.

[44] One caveat here also is that the threshold theories developed in this paper are only applicable for soil mantled hillslopes. The linkage between vegetation and geomorphic processes is lead by soil production. In many cases, at high uplift rates, soil production may not keep up with erosion by landsliding, exposing the bedrock. Incorporating a soil production function in our analysis would set an upper limit to the uplift rate in our framework, above which no soil would be available for erosion.

5. Morphologic Implications of Vegetation on the Landscape: Modeling Experiments

[45] The analytic theory described above provides some indication of how vegetation may control the dominant erosion processes at the valley head, and resulting drainage density. An ideal approach to explore the long-term consequences of vegetation-erosion dynamics on landscape morphology is through the use of numerical modeling of basin evolution. This way, factors neglected in the analytical solutions, such as stochastic climate forcing, vegetation death and regrowth, effects of slope divergence and convergence on the soil creep transport as well as the nonlinear soil creep model can be explicitly considered, and their influence on the landscape structure can be investigated. Here we present four simulation experiments conducted using the CHILD model [*Tucker et al.*, 2001b, 2001c; *Tucker and Bras*, 2000]. We first describe the dynamic vegetation model employed in this study followed by the simulation experiments.

5.1. Dynamic Vegetation Model

[46] The rate of vegetation colonization is modeled using the well-known growth function proposed by *Levins* [1969]:

$$\frac{dV}{dt} = \frac{1}{T_g} V(1 - V) - \frac{1}{T_m} V, \tag{31}$$

where dV/dt is the rate of change in vegetation cover fraction, T_g is a growth timescale that describes the time required for vegetation to grow on bare soil under no limitations for resource and reproductivity, and T_m is a mortality timescale. Note here that $1/T_g$ and $1/T_m$ are equivalent to intrinsic colonization and mortality rates described in the original form of this population growth model [*Levins*, 1969; *Tilman*, 1994]. Two important implications of this model are (1) water and nutrients do not limit vegetation growth and (2) vegetation only competes for space to establish new sites. The colonization rate, $(1/T_g)V$, increases as vegetation becomes denser, due to

the availability of seeds and dispersal sources. Multiplying the colonization rate with the available space unoccupied by vegetation gives the rate of growth in newly colonized sites [*Tilman*, 1994]. The mortality term, $(1/T_m)V$ gives the rate at which sites become vacant. Vegetation growth approaches zero either when the cover is dense, or very sparse. In the former case it is the space that limits the growth, whereas in the latter, sources for reproduction. Vegetation cover attains an equilibrium cover when $dV/dt = 0$, which gives the maximum cover fraction as, $V_{\max} = 1 - T_g/T_m$. Integrating equation (31) with respect to time gives vegetation cover, growing from an initial cover fraction at time = 0, as a function of time:

$$V(t) = \frac{V_o V_{\max}}{V_o + (V_{\max} - V_o)e^{-T' V_{\max}}}, \tag{32}$$

where V_o is the initial vegetation cover for vegetation growth, and T' is a nondimensional growth timescale, $T' = t/T_g$, where t is time. As indicated before, this equation assumes no limitations in resources such as water, and therefore may be appropriate for vegetation modeling in humid climates. In water limited ecosystems, both vegetation colonization and mortality rates may be affected by soil moisture [*Fernandez-Illescas and Rodriguez-Iturbe*, 2004].

[47] In addition to mortality, we model vegetation death by runoff erosion and landsliding, as these processes remove the substrate for vegetation, and wildfires. The rate of vegetation destruction by overland flow is logically a function of excess shear stress and vegetation cover available on the surface [*Tucker and Bras*, 1998; *Collins et al.*, 2004]. In the case of shallow landsliding, vegetation removal rate essentially becomes infinite as most landslides scour regolith to bedrock:

$$\frac{dV}{dt} = \begin{cases} -k_v V(\tau_f - \tau_c), & \tau_f > \tau_c : \text{erosion} \\ -\infty, & S > S_c : \text{landslides} \end{cases}, \tag{33}$$

where k_v is vegetation erodibility parameter.

[48] Arrival of spatially uniform wildfires in the model resembles a Bernoulli process with equal probability of fires occurring each year. The model predicts a wildfire when a uniformly distributed random number between 0 and 1 generated for each year is greater than or equal to the probability that a fire does not occur in a given year, P_F, calculated using the mean time between fires, $\bar{T}_F$:

$$\text{Rnd}(\text{Uniform} \sim [0,1]) \geq P_F(\bar{T}_F \leq T_F) = \frac{\bar{T}_F - 1}{\bar{T}_F}, \tag{34}$$

where Rnd(U) is a uniformly distributed random number. Fires are assumed to kill all the vegetation in the modeled domain. Because wildfire arrival is independent of the vegetation cover, this model is more applicable to conditions where wildfires are weather related and driven by lightning strike. In some environments, especially where summers are dry, wildfires may cause water repellent conditions on the soil surface [*Gabet and Dunne*, 2003a]. Water repellency may significantly increase runoff rates, triggering extensive gully erosion [*Meyer and Wells*, 1997; *Meyer et al.*, 2001; *Istanbulluoglu et al.*, 2004]. In the simulation experiments we forced the model using climate statistics from Oregon, where fire related water repellence is not a concern [*Benda and Dunne*, 1997]. Therefore water repellence and other potential effects of wildfires on hillslope hydrology are neglected in this study.

[49] It is perhaps important to recognize here that effects of wildfires on the vegetation cover could be different from floods. In modeling flood-driven plant disturbances, we assumed that when erosion occurs it disturbs both surface vegetation cover and its roots simultaneously. This assumption can be justified because erosion removes the substrate that supports both surface and subsurface vegetation components [*Hack and Goodlett*, 1960]. Fires have a slightly different consequence on landscape vegetation. While surface vegetation cover burns during the fire, root strength usually diminishes within the next decade following the fire [*Burroughs and Thomas*, 1977; *Sidle*, 1992]. Therefore depending on other factors such as climate forcing, significant runoff erosion may be observed immediately after the fire, while landsliding usually starts within the first decade [*Megahan et al.*, 1978; *Gray and Megahan*, 1981; *Istanbulluoglu et al.*, 2004]. Decay in the root cohesion is modeled using a relationship similar to that used by *Burroughs and Thomas* [1977] and *Sidle* [1992]:

$$C'_{rd} = C'_r V_o \exp(-At^B), \tag{35}$$

where C'_r is root cohesion provided by mature plants normalized to soil weight (e.g., equation (20)), V_o is the initial vegetation cover at the time of fire that is subject to death, and A and B are empirical parameters. In modeling landslide initiation following a wildfire, cohesion imparted by decaying roots is added to the cohesion produced by the regenerating vegetation in equation (20).

5.2. Simulation Experiments

[50] In all the simulations reported in this section, climate is driven by the rectangular Poisson pulse model. In its simplest form, storm intensity, p, storm duration, t_r, and interstorm period, t_b, are independent random variables described by an exponential distribution function [*Eagleson*, 1978]:

Storm intensity

$$f_P(p) = \frac{1}{\bar{p}} \exp\left(-\frac{p}{\bar{p}}\right), \tag{36a}$$

Storm duration

$$f_{T_s}(t_s) = \frac{1}{\bar{t}_s} \exp\left(-\frac{t_s}{\bar{t}_s}\right), \tag{36b}$$

Time between storms

$$f_{T_b}(t_b) = \frac{1}{\bar{t}_b} \exp\left(-\frac{t_b}{\bar{t}_b}\right). \tag{36c}$$

The rectangular Poisson pulse model has been used in recent studies of modeling landscape evolution [*Tucker and Bras*, 2000; *Tucker*, 2004; *Collins et al.*, 2004] and ecohydrology [*Eagleson*, 2002].

[51] We force the model by storms and tectonic uplift, both representative of the Oregon Coast Range (OCR). In

Table 1. Model Parameter Values Used in Simulations

Parameter	Value
Uplift (U), mm/yr	0.25
Mean storm intensity ($\bar{p}$), mm/h	0.68
Mean storm duration ($\bar{t}_r$), hours	31.5
Mean time between storms ($\bar{t}_b$), hours	148
Soil erodibility (k_e), m yr^{-1} (kg m^{-1} s^{-2})$^{-p}$	0.1
Critical shear stress for soil erosion, kg m^{-1} s^{-2}	1
Roughness coefficient for bare surface (n_b)	0.025
Diffusivity constant (K_b), m^2/yr, and exponent (α)	0.01, 1
Normalized root cohesion (C'_r)	0.7
Soil friction angle (ϕ), deg	35
Hydrology parameter (Γ)	0.002
Vegetation growth timescale (T_g), years	10
Vegetation mortality timescale (T_m), years	200
Vegetation erodibility (κ), yr^{-1} kg^{-1} ms	1
Roughness coefficient for mature vegetation (n_{VR})	0.6
Root strength parameters for decay (A, B), yr^{-1}	0.5, 0.73
Mean time between fires ($\bar{T}_F$), years	200

this area, climate is characterized by long-duration, low-intensity rainfall events typical of Pacific storm systems that show small seasonal fluctuations. *Hawk* [1992] reports the parameters of the rectangular Poisson pulse model monthly for 75 stations throughout the United States, including one in the state of Oregon. We neglect seasonality in the precipitation and used the averages of the mean monthly values for rainfall rate, interstorm duration and storm duration from *Hawk* [1992]. In the OCR, erosion is argued to be in approximate equilibrium with rock uplift [*Reneau and Dietrich*, 1991; *Kelsey and Bockheim*, 1994; *Personius*, 1995]. We used an uplift rate of 0.25 mm/yr, in the range of the reported values in the literature. For the roughness coefficients of bare soil and vegetation cover, we use the numbers we have given in section 3 for grass, based on the data of *Prosser et al.* [1995]. These and other parameter values used in the simulations are listed in Table 1.

[52] The initial domain for the model simulations is a 700 m by 700 m inclined surface with a 40% slope constructed by Voronoi polygons of 15 m node spacing. Drainage is only permitted through one side of the domain. We neglect infiltration, and calculate steady–state discharge at each point as the product of the total drainage area of each cell and the rainfall rate, $q = pA$. In modeling landslide initiation, we use a deterministic hydrology parameter, Γ (P/T) in equation (21) (Table 1). Two reasons for this are: first, subsurface flow often does not attain steady state during individual storms, and has a slower, aggregated response to stochastic storms [e.g., *Barling et al.*, 1994; *Borga et al.*, 2002]. Consistent with the relatively slow response of subsurface flow to storm forcing, a number of researchers have used deterministic hydrology parameters to map ground saturation and landslide initiation, confirmed by field observations in the western U.S. [*Dietrich et al.*, 1993; *Montgomery and Dietrich*, 1994; *Istanbulluoglu et al.*, 2002]. Second, a constant hydrology parameter allows the isolation of the effects of vegetation and erosion interactions on the landscape morphology by reducing the uncertainty in the topographic signature of landsliding [i.e., *Tucker and Bras*, 1998].

[53] In applying the nonlinear hillslope diffusion model we calculate the threshold slope parameter, S_c using equation (20), ignoring the effects of pore pressure ($\Gamma = 0$) on disturbance driven shallow soil slips [*Roering et al.*, 1999]. Pore pressure activated shallow landsliding is modeled when the critical slope, calculated using equation (20) in each model iteration, is smaller than the local slope. Eroded material at the landslide scarp is assumed to leave the basin without any deposition. No deposition is allowed for material removed by fluvial erosion, and soil loss by wash processes is assumed to depend only on local effective shear stress. This has some justification, as erosion is very limited on vegetated hillslopes even under large floods owing to the protection provided by plants [*Prosser et al.*, 1995]. Baseline hillslope diffusivity is assumed to be 0.01 m^2/yr, in agreement with estimated diffusion rates in humid environments [e.g., *Roering et al.*, 2002]. In relating vegetation to hillslope diffusivity we used $\alpha = 1$. For maximum vegetation cover $V_{\max} = 0.95$, and $\alpha = 1$, equation (17) predicts a diffusion constant of $K_d = 0.0039$. This number is within the range of diffusion constants estimated by *Roering et al.* [1999] in a number of small watersheds in the OCR using topographic data.

[54] The first two simulations consider the end member cases: bare soil, and full vegetation cover on the landscape, with no vegetation disturbances driven by floods, erosion or fires. Though not realistic, using a static vegetation cover

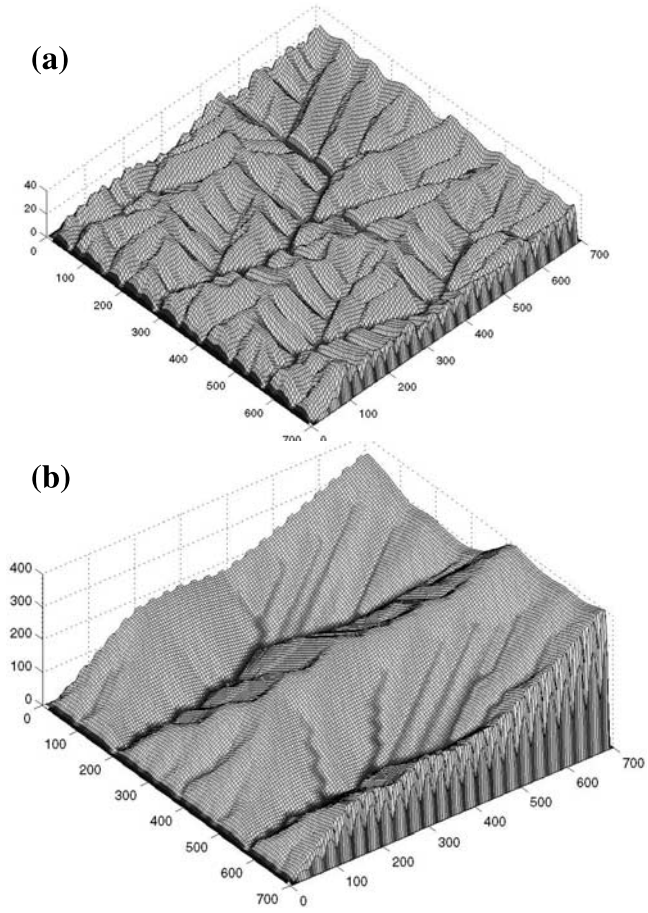

Figure 6. Numerical simulations illustrating the contrasting difference in the landscape morphology with (a) no vegetation cover and (b) static vegetation cover. Both landscapes are in dynamic equilibrium, with mean elevations subject to fluctuations about a long term mean due to stochastic climate forcing and static erosion thresholds.

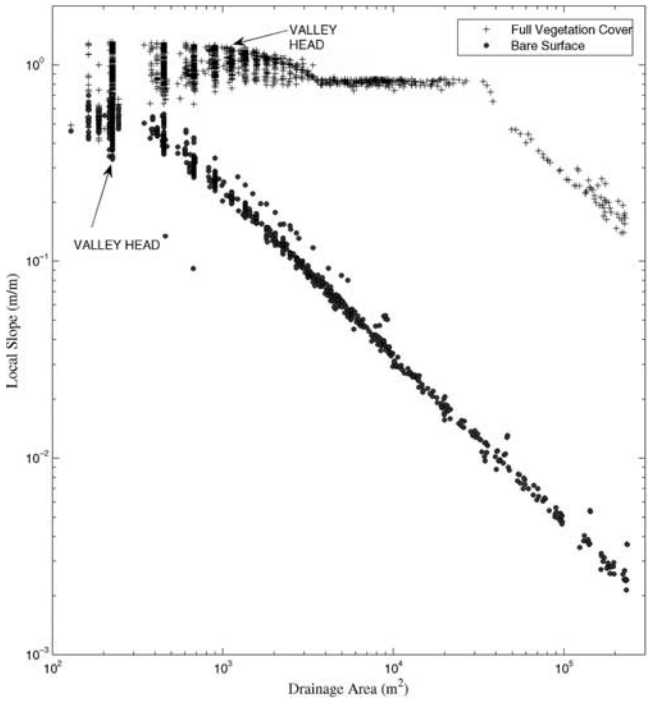

Figure 7. Relationship between local slope and drainage area for simulated landscapes with full vegetation cover and bare soil.

isolates the effects of vegetation disturbances on the development of landscape morphology. Topographies simulated under these conditions are shown in Figure 6, and their corresponding slope-area diagrams in Figure 7. Both basins are eroding at an identical mean rate, approximately equal to the constant, spatially uniform, rate of tectonic uplift. Striking differences in the landscape structure between the two reveal the importance of vegetation in landscape evolution.

[55] In the absence of vegetation, runoff shear stress is fully exerted on the soil surface, and with a low soil detachment threshold, storms generate frequent erosion, even in the upper portions of the simulated catchment. The effectiveness of fluvial erosion forms a highly dissected, low-relief topography (Figure 6a) typical of unvegetated landscapes with highly erodible soils [*Howard*, 1997; *Collins et al.*, 2004]. In this simulation, the hillslope-valley transition occurs where the rate of soil removal by runoff erosion is higher than infilling by hillslope diffusion (Figure 7). This scale also marks the transition from near-planar hillslopes to concave valleys that yields a turnover point on the slope-area data of the simulated topography [*Tarboton et al.*, 1992; *Howard*, 1994; *Moglen and Bras*, 1995]. In the contrasting case, static vegetation that fully occupies the land surface seals the soil surface to runoff erosion almost entirely, and significantly reduces physical soil creep processes. Continuing uplift under this condition increases the elevations until slopes exceed the critical threshold for landsliding (equation (20)), and hillslope erosion is predominantly by mass wasting. This difference in the dominant denudation process is reflected on the slope area diagram, where the slope stability envelop exhibits an upper limit to slope steepening (Figure 7) [*Montgomery and Dietrich*, 1994; *Tucker and Bras*, 1998]. In the slope area space, portions of the landscape with low drainage area represent a combination of diffusion and unsaturated landsliding. As area increases, elevated pore pressure driven by subsurface flow reduces the landsliding threshold (equation (20)), triggering mass failures that lower local elevations, producing slope convergence. Theory for form instability predicts valley formation when the equilibrium gradient decreases with increasing contributing area [*Smith and Bretherton*, 1972; *Tarboton et al.*, 1992; *Tucker and Bras*, 1998]. In this sense, the rounding portion of the slope stability envelope corresponds to locations in Figure 6b where hollows form. With full soil saturation, threshold slope is independent of contributing area and plots as a horizontal line on the slope-area diagram. This flat region extents to the point where the threshold gradient for landslides is equal to the equilibrium gradient for water erosion, below which concave channels begin. The topographic features of these processes can be clearly seen in Figure 6b, with straight channels draining large hillslope segments, and integrating into a slightly more tortuous channel system in the valley bottoms. Comparing the fluvial sections of both simulations in Figure 7, for a given contributing area, equilibrium slopes are significantly, up to five orders of magnitude, larger in the vegetated landscape than in the bare. One caveat here is that debris flow erosion is not explicitly modeled in this study. It has been argued that in steep, soil-mantled landscapes debris flows triggered by landslide activity may dominate erosion in headwater channels leaving their signatures on the slope-area space. Debris flow channels usually exhibit a power law relationship between slope and area, less steep than fluvial scaling, with gradual transition to purely fluvial scaling [*Montgomery*, 2001; *Stock and Dietrich*, 2003; *Kobor and Roering*, 2004]. Debris flow behavior on complex terrain involves physical processes that integrate sediment and wood, each behaving differently [*May*, 2002; *Lancaster et al.*, 2003]. Bearing in mind that debris flow processes may have some effect on the simulations, we will leave this detail to future research due to current limitations in their mechanistic understanding. A last remark relative to the simulations discussed here is that, despite the fact that the model parameters are selected to be representative of the OCR, none of the two simulated basins in Figure 6 resembles typical OCR topography, a steep, high-relief and highly dissected morphology with relatively uniform gradient hillslopes formed under the action of shallow landsliding [e.g., *Roering et al.*, 1999, Figure 1]. We would argue that this is due to the unrealistic states assumed for the vegetation cover.

[56] In the third simulation, we model vegetation disturbances by runoff erosion and landsliding. A finite rate for vegetation destruction by erosion is computed according to equation (33), when the effective shear stress is higher than the critical shear stress. Landslides are assumed to disrupt all the vegetation cover instantaneously as the denudation rate is effectively infinite during mass failures. Parameters of the vegetation growth model are selected such that approximately 80% of the vegetation cover reestablishes in 50 years following a disturbance, a reasonable time frame for the regeneration of most forests in the western US [*Sidle*, 1992]. Simulated topography under this scenario is plotted in Figure 8, and its slope-area relationship in Figure 9. In

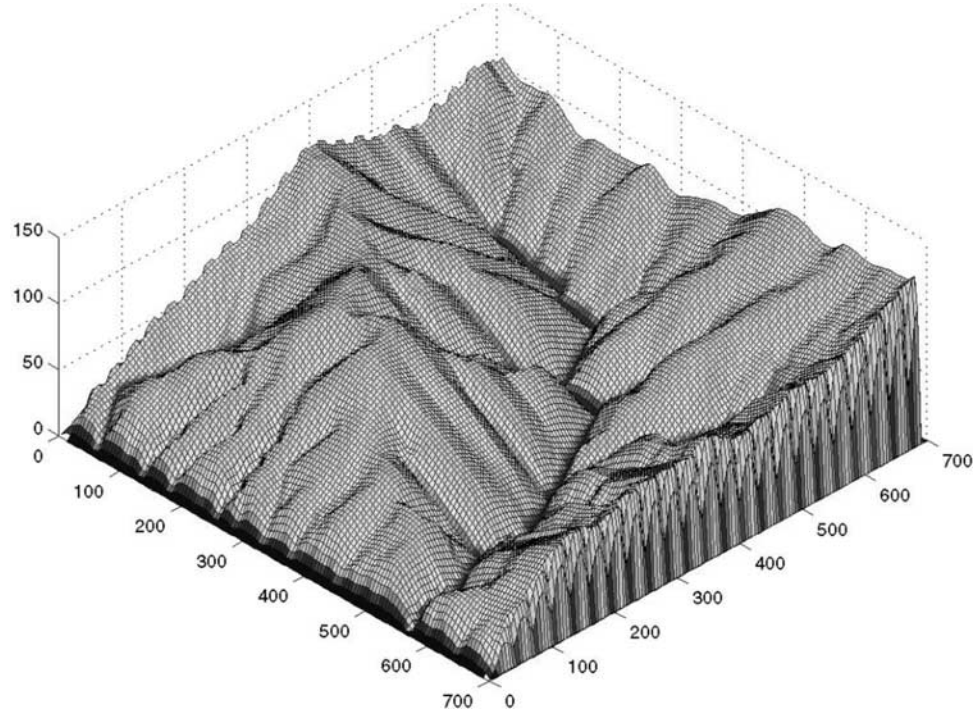

Figure 8. Simulated landscape with dynamic vegetation cover. Vegetation grows as a function of available space and vegetation cover and is disrupted by water erosion and landsliding.

this simulation, the landscape in equilibrium is subject to fluctuations in the local elevations, given the stochastic storm forcing, and the increased erosion rates following vegetation disturbances [*Collins et al.*, 2004]. None of these effects significantly alter the large-scale basin morphology, nor the process signatures in slope area space, therefore they are not further discussed here. What this simulation shows is clearly the effect of dynamic vegetation cover on landscape development. Compared to the static vegetation simulation (Figure 6b), the outcome of vegetation-erosion coupling is a more highly dissected topography, with smaller landslide-dominated hollows entering the channel network with higher junction angles and a more tortuous channel network. Mean elevation is approximately three times smaller than that of the static vegetation simulation.

[57] The slope–area data of the simulated topography show significant scatter and are bounded by the slope area relationships of the bare and static vegetation runs. In this simulation, landslide-dominated hollows erode in a self-driven cycle of slope steepening in the hollow axis due to continuing tectonic uplift and sediment infilling, and consequent landsliding [*Dietrich et al.*, 1986]. During the steepening phase, hillslope gradients may increase up to the threshold gradient imposed by the slope stability envelope of the vegetated landscape (Figure 9). Removal of soil and vegetation by landsliding reduces local slopes to a stable threshold gradient. This creates a base level drop for the areas upstream, and depending on the vegetation cover, and storm arrivals, may trigger significant upland erosion. In addition, exceptional storms may disrupt the vegetation cover, reducing thresholds for both landsliding and water erosion, triggering extensive erosion. Increases in diffusion rates during the times when hillslopes are devegetated also results in shallower gradients on hillslopes. Both in hillslope and channel portions, slopes are lower than for the fully vegetated landscape on average. Note also the reduction in the basin size, in addition to slopes, where fluvial erosion starts outweighing landsliding on the slope-area diagram (Figure 9).

[58] Loss of surface vegetative cover and root cohesion following stand-replacing wildfires may trigger catastrophic geomorphic response [e.g., *Meyer et al.*, 2001]. Some

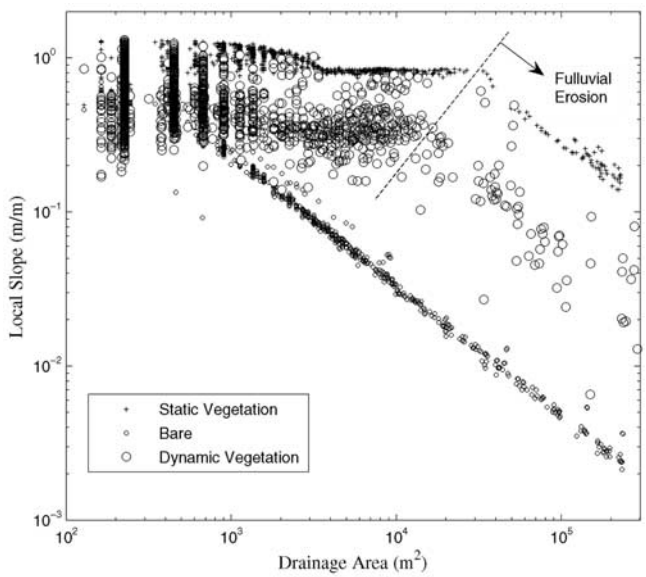

Figure 9. Relationship between local slope and drainage area for the simulated landscape pictured in Figure 8, plotted with the slope-area data of bare and static vegetation simulations.

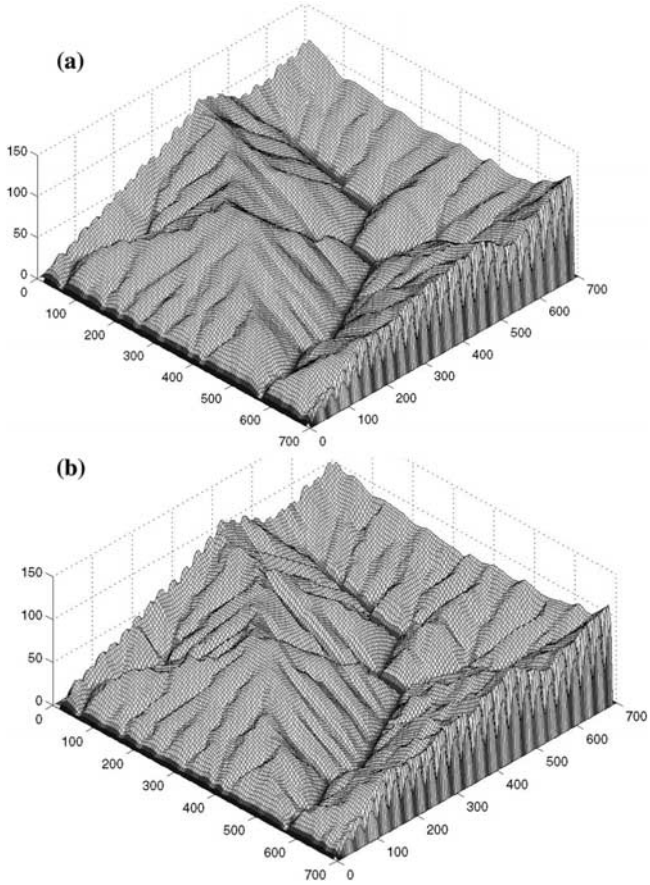

Figure 10. Effects of wildfires on the simulated landscape: (a) landscape that has the maximum amount of mass during the 600,000-year-long simulation and (b) landscape with the minimum mass during the simulation.

modeling studies have argued that over millennial timescales erosion frequency and magnitude in space is closely related to random sequences of wildfires and storm forcing [*Benda and Dunne*, 1997; *Istanbulluoglu et al.*, 2004]. It is also conceivable that by altering erosion rates and timing, wildfires influence landscape morphology. To test this hypothesis, we submit the landscape pictured in Figure 8 to wildfires arriving randomly with a mean return interval of 1 in 200 years, a rate within the reported range for the Quaternary average fire intervals in the western US based on charcoal deposits [*Long*, 1995; *Karsian*, 1995].

[59] Using the landscape in Figure 8 as the initial condition, the model is run forward for 600,000 years with random fires. To show the potential influence of fires on the landscape morphology, we picture two end member landscapes in Figure 10, with maximum (Figure 10a) and minimum (Figure 10b) landscape mass during the 600,000 years of simulation under fire disturbances. The top figure is a landscape after a period of quiescence, where in the last 12,000 years tectonic uplift caused a net 1.5 meter increase in the mean basin elevation. This period is followed by a period of accelerated erosion that lasts about 8,000 years, in which combination of fires and random storm arrivals on oversteepened hillslopes produced massive denudation. Figure 10b corresponds to the end of this accelerated erosion period where sediment in almost all the depressions are evacuated, and a number of additional hollows have been incised by erosion and mass failures. This activity has reduced the mean basin elevation 2 meters in 8000 years, accounting for an average denudation rate of 0.5 mm/yr (including the steady state uplift), twice the uplift rate used in the simulation.

[60] Because fire-induced loss in surface resistance occurs uniformly everywhere in the model, erosion and mass movements mostly concentrate during periods of low erosion thresholds. The landscape responds to fire related increase in erosion activity by slightly reducing the local slopes to compensate for the same fixed rate of uniform tectonic uplift. Therefore fires cause approximately a 7% decrease in the spatial mean of the basin elevations (difference between Figures 9 and 10a) as the basin reaches its new state of dynamic equilibrium, resulting in reductions in the number of steep landscape segments in the slope-area diagram (compare Figure 11 with Figure 9).

[61] Even though the landscape shown in Figure 10a is in a rising state with hollows infilled with colluvium after the last cycle of hollow evacuation (not pictured), two apparent signatures of past wildfire-induced erosion activity, compared to Figure 8, are increased drainage density and reduced basin relief. In the slope area plot of the landscape evolved without fire disturbance (Figure 9), slopes start exhibiting a decreasing trend with drainage area for source areas greater than 400 m^2 which sets the average size of a zero-order basin for this landscape. In the case of fires, average zero-order basin size is approximately 200 m^2 (Figure 11), and becomes smaller after the basin-wide erosion activity with channel heads eroding up to ridge tops (Figure 10b).

[62] Hillslopes tend to be less steep under fire disturbance, for two reasons. First, after the fires, before the establishment of surface vegetation, hillslope diffusion rates suddenly increase as the hillslope diffusivity constant increases (equation (17)) and the threshold gradient for

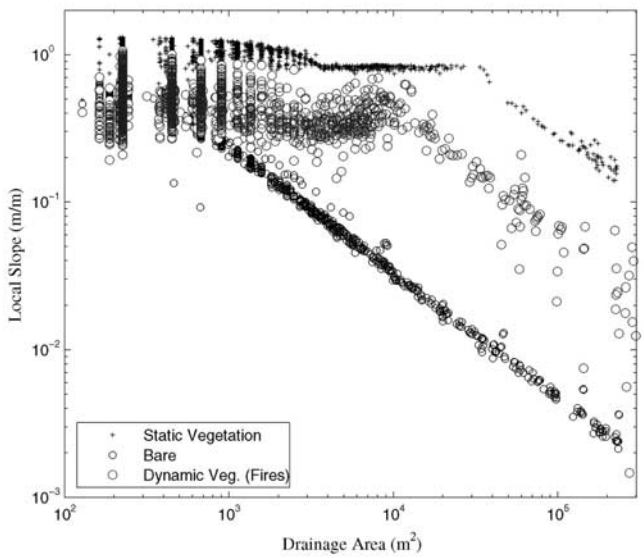

Figure 11. Relationship between local slope and drainage area for the simulated landscape pictured in Figure 10a, plotted with the slope area relationships of bare and static vegetation simulations.

sliding, S_c decreases with vegetation loss. Second, with wildfires, the landscape spends longer times under the influence of smaller root cohesion owing to the cycles of root decay and regrowth driven by the random arrival of wildfires. When integrated over long time periods, these fluctuations in the root cohesion sets a lower threshold gradient for pore pressure–driven landsliding. Simultaneous death of vegetation with fires, and spatially invariable growth rates reduces the spatially diversity in the vegetation cover, resulting in less scatter in the slope-area data. Note also that in Figure 11, the slight increase in the slopes, immediately before the onset of fluvial scaling is produced by the competition between fluvial erosion that imposes a higher equilibrium slope gradient as contributing area decreases, than the threshold slope imposed by landsliding (Figure 11). These points correspond to locations toward the lower segments of landslide-dominated hollows, slightly upstream of points where hollows connect with the fluvial network.

6. Conclusions

[63] We have investigated the implications of static and dynamic vegetation cover on geomorphic processes and resulting landforms using quantitative theory and numerical modeling. Analytical expressions developed to quantify channel head source area size for runoff erosion and landsliding for hillslopes in equilibrium, exhibit a complex response to changes in the vegetation cover. In the simplest case, when vegetation does not influence hillslope diffusion, source area is positively related to vegetation cover as a response to reduced efficiency of flow shear stress and increased slope-area threshold for landsliding. This implies a negative relationship between drainage density and vegetation cover. According to the theory, drainage density under runoff erosion may be more sensitive to vegetation cover than that determined by landsliding. When vegetation inhibits hillslope diffusion, our model suggests that source area may increase or decrease depending on the relative influence of vegetation in altering the diffusion rates. A reduction in the source area (or increase in drainage density) with increasing vegetation cover occurs when hillslope gradients tend to steepen rapidly to cope with the constant rate of tectonic uplift under reduced hillslope diffusivity caused by vegetation. Here, an increase in the local slope implies a reduction in the threshold area to provide a fixed shear stress or pore pressure threshold for channel initiation.

[64] Using reasonable parameters to characterize vegetation and soil resistance to erosion and landsliding, we show analytically, for end-member cases of high and low U_* (uplift to diffusivity ratio), that the channel head is formed by landsliding when U_* is high and by runoff erosion when U_* is low. While vegetation influences the size of the source area and drainage density, the type of the dominant process at the channel head is not controlled by vegetation, suggesting that U_* plays a decisive role in the dominant geomorphic process that forms channels in these end member cases. However when U_* has a moderate value, vegetation cover controls the type of the erosion process at the channel head. The theory suggests that a runoff erosion–dominated landscape under poor vegetation cover may be landslide dominated under a denser cover.

[65] We do not know of studies that correlate drainage density solely to vegetation cover, as climate often controls the distribution of plants on the landscape. Notable contributions relate drainage density inversely to climate [*Melton*, 1957], or suggest that D_d increases with precipitation under arid and semiarid climates, reaches a maximum, and decreases with more humid conditions [*Gregory and Gardiner*, 1975]. To the extent that these studies reflect the control of vegetation on drainage density, relationships between drainage density and vegetation cover predicted by the analytic theory developed in this paper are in agreement with the data of *Melton* [1957] when hillslope creep rates are not influenced by vegetation ($\alpha = 0$). If vegetation impedes soil creep rates, as some field observations suggested [*Young*, 1972; *Selby*, 1974; *Jahn* 1981, 1989; *Alberts et al.*, 1995; *Malmon and Dunne*, 1996], the model predicts an upward concave relationship between vegetation cover and drainage density when (1) channel head source area is controlled by runoff erosion, or (2) there is a vegetation-modulated transition from runoff erosion to landsliding at the channel head (intermediate and low U_* in Figure 5). This shape is opposite to the bell-shaped relationship between precipitation and drainage density of *Gregory and Gardiner* [1975]. If, however, hillslope diffusion increases with vegetation cover as other field studies indicate [*Roering et al.*, 2002; *Black and Montgomery*, 1991; *Nash*, 1980] because of enhanced bioturbation, then the model would potentially predict a downward concave relationship between vegetation and drainage density, in agreement with the data. However it is important to bear in mind that the data of *Gregory and Gardiner* [1975] reflect not only the effects of vegetation, but also potential differences in the erosivity on the drainage density under different climates. Thus an attempt to describe *Gregory and Gardiner*'s [1975] data would require an elaborate theory that couples vegetation and erosion dynamics with climate. Because, to our knowledge, there is no systematic field evidence that relates soil creep to vegetation cover or climate, in this study we used the existing models that related soil creep rates negatively to vegetation cover [*Alberts et al.*, 1995; *Malmon and Dunne*, 1996]. It is conceivable that creep rates have a minimum value at some intermediate vegetation cover and increase toward both higher and lower values of coverage, yielding a U-shaped relationship (J. Roering, personal communication, 2005). While the simple exponential model used in this study does not represent the effects of various soil creep processes in the continuum from bare ground to forest, nevertheless understanding the long-term implications of some of them is still a valuable contribution.

[66] We have performed four numerical experiments using the CHILD model, with parameter values for tectonic and climate forcing, vegetation and soils representative of the Oregon Coast Range (OCR). Simulated surface cover conditions include: bare soil, static vegetation, and dynamic vegetation cover which is subject to geomorphic disturbances in one simulation, and both geomorphic and wildfire disturbances in another. The bare landscape evolves under the action of fluvial erosion forming a highly dissected topography typical of badlands [*Howard*, 1997]. In the other extreme end, with static vegetation cover, the landscape is landslide dominated, consisted of mostly planar hillslopes,

has a higher relief and a significantly lower drainage density. In this example, because water erosion is very rare under vegetation cover, continuing uplift and consequent slope steepening brings slopes to a point that they predominantly erode by landsliding. This is consistent with the experimental flume studies of Prosser and coworkers [*Prosser et al.*, 1995; *Prosser and Dietrich*, 1995] who concluded that the thresholds imparted by natural vegetation in their study area were so high that channels could only initiate under unrealistic rainfall rates. Thus for erosion to keep up with uplift rates, landsliding-dominated valleys develop, as was the case in our simulation. In addition, natural or anthropogenic vegetation disturbances at some random intervals provide conditions for channel initiation by runoff erosion and landsliding that may result in episodic hollow evacuation [*Prosser and Dietrich*, 1995; *Benda and Dunne*, 1997].

[67] The model underscores the fundamental importance of the type and frequency of vegetation disturbances on the landscape morphology. Vegetation disturbances by runoff erosion and landsliding, both driven by random storms, contribute to the formation of a highly dissected topography, which has a significantly lower relief than the landscape evolved under static vegetation. Imposing fires with an arrival rate of 1 in every 200 years further increased landscape dissection and reduced relief. Topography simulated under vegetation disturbances closely resembles natural landscapes in the OCR where vegetation disturbances by fires and floods are common [*Lancaster et al.*, 2003].

[68] Our numerical experiments reveal the importance of vegetation on landscape evolution. We foresee two potential avenues of research in understanding the controls of climate and vegetation in geomorphic processes: (1) an improved process-based understanding of the effects of vegetation on geomorphic transport laws and (2) dynamic coupling between climate, soil moisture, vegetation growth and erosion. Although the former is under examination in both humid [*Schmidt et al.*, 2001; *Roering et al.*, 2003] and semiarid climates [*Abrahams et al.*, 1995; *Puigdefábregas and Sánchez*, 1996], the latter still remain to be explored, and is in the research prospect of the authors.

[69] **Acknowledgments.** This work is funded by the U.S. Army Research Office contract number DAAD19-01-1-0513 and by the Italian National Research Council. We thank Daniel Collins for directing us to some of the literature used in the introduction section of the paper. This work has benefited from thoughtful reviews by Joshua J. Roering and Alex Densmore.

References

Abe, K., and R. R. Ziemer (1991), Effect of tree roots on shallow-seated landslides, *USDA For. Serv. Gen. Tech. Rep.*, *130*, 11–20.

Abrahams, A. D., and A. J. Parsons (1994), Hydraulics of interill overland flow on stone-covered desert surfaces, *Catena*, *23*, 111–140.

Abrahams, A. D., A. J. Parsons, and J. Wanwright (1995), Effects of vegetation change on interrill runoff and erosion, Walnut Gulch, southern Arizona, *Geomorphology*, *13*, 37–48.

Alberts, E. E., M. A. Nearing, M. A. Weltz, L. M. Risse, F. B. Pierson, X. C. Zhang, J. M. Laflen, and J. R. Simanton (1995), Soil component, in *USDA—Water Erosion Prediction Project*, *Rep. 10*, pp. 7.1–7.47, Natl. Soil Erosion Res. Lab., West Lafayette, Ind.

American Society of Civil Engineers (1996), Hydrology handbook, *Manuals Rep. Eng. Prac. 28*, 2nd ed., 784 pp., New York.

Arnold, J. G., M. A. Weltz, E. E. Alberts, and D. C. Flanagan (1995), Plant growth component, in *USDA—Water Erosion Prediction Project*, *Rep. 10*, chap. 8, pp. 8.1–8.41, Natl. Soil Erosion Res. Lab., West Lafayette, Ind.

Barling, R. D., I. D. Moore, and R. B. Grayson (1994), A quasi-dynamic wetness index for characterizing the spatial distribution of zones of surface saturation and soil water content, *Water Resour. Res.*, *30*, 1029–1044.

Benda, L., and T. Dunne (1997), Stochastic forcing of sediment supply to channel networks from landsliding and debris flow, *Water Resour. Res.*, *33*, 2849–2863.

Black, T. A., and D. R. Montgomery (1991), Sediment transport by burrowing animals, Marin County, California, *Earth Surf. Processes Landforms*, *16*, 163–172.

Borga, M., G. D. Fontana, and F. Cazorzi (2002), Analysis of topographic and climatic control on rainfall-triggered shallow landslides using a quasi-dynamic wetness index, *J. Hydrol.*, *268*, 56–71.

Burroughs, E. R., and B. R. Thomas (1977), Declining root strength in Douglas-fir after felling as a factor in slope stability, *USDA For. Serv. Res. Pap. INT-190*, 27 pp., For. and Range Exp. Stn., Ogden, Utah.

Carson, M. A., and M. J. Kirkby (1972), *Hillslope Form and Processes*, Cambridge Univ. Press., New York.

Collins, D. B. G., R. L. Bras, and G. E. Tucker (2004), Modeling the effects of vegetation-erosion coupling on landscape evolution, *J. Geophys. Res.*, *109*, F03004, doi:10.1029/2003JF000028.

Cotton, C. A. (1955), *New Zealand Geomorphology*, 281 pp., N. Z. Univ. Press, Wellington.

Davis, F. W., E. A. Keller, A. Parikh, and J. Florsheim (1989), Recovery of the chaparral riparian zone after wildfire, *For. Serv. Gen. Tech. Rep. PSW-110*, pp. 194–203, U.S. Dept. of Agric., Washington, D. C.

Dietrich, W. E., C. J. Wilson, and S. L. Reneau (1986), Hollows, colluvium and landslides in soil-mantled landscapes, in *Hillslope Processes*, edited by A. Abrahams, pp. 361–388, Allen and Unwin, St Leonards, NSW, Australia.

Dietrich, W. E., C. J. Wilson, D. R. Montgomery, and J. McKean (1993), Analysis of erosion thresholds, channel networks, and landscape morphology using a digital terrain model, *J. Geol.*, *101*, 259–278.

Dunne, T. (1990), Hydrology, mechanics, and geomorphic implications of erosion by subsurface flow, *Spec. Pap. Geol. Soc. Am.*, *252*, 1–28.

Eagleson, P. S. (1978), Climate, soil and vegetation: 2. The distribution of annual precipitation derived from observed storm sequences, *Water Resour. Res.*, *14*, 713–721.

Eagleson, P. S. (2002), *Ecohydrology: Darwinian Expressions of Forest Form and Function*, 443 pp., Cambridge Univ. Press, New York.

Einstein, H. A., and N. L. Barbarossa (1952), River channel roughness, *Trans. Am. Soc. Civ. Eng.*, *117*, 1121–1132.

Engelund, F., and E. Hansen (1967), *A Monograph on Sediment Transport in Alluvial Streams*, 62 pp., Teknisk Vorlag, Copenhagen.

Engman, E. T. (1986), Roughness coefficients for routing surface runoff, *J. Irrig. Drainage Eng.*, *112*, 39–53.

Fernandez-Illescas, C. P., and I. Rodriguez-Iturbe (2004), The impact of interannual rainfall variability on the spatial and temporal patterns of vegetation in a water-limited ecosystem, *Adv. Water Res.*, *27*, 83–95.

Florinsky, I. V., and G. A. Kuryakova (1996), Influence of topography on some vegetation cover properties, *Catena*, *27*, 123–141.

Foster, G. R. (1982), Modeling the erosion process, in *Hydrologic Modeling of Small Watersheds*, *ASAE Monogr.*, vol. 5, edited by C. T. Haan, pp. 295–380, Am. Soc. Agric. Eng., St. Joseph, Mo.

Foster, G. R., L. F. Huggins, and L. D. Meyer (1968), Simulation of overland flow on short field plots, *Water Resour. Res.*, *4*, 1179–1187.

Foster, G. R., D. C. Flanagan, M. A. Nearing, L. J. Lane, L. M. Risse, and S. C. Finkner (1995), Hillslope erosion component, in *USDA-Water Erosion Prediction Project*, *Rep. 10*, pp. 11.1–11.12, Natl. Soil Erosion Res. Lab., West Lafayette, Ind.

Freeman, G. E., W. J. Rahmeyer, and R. R. Copelan (2000), Determination of resistance due to shrubs and woody vegetation, *Rep. ERDC/CHL TR-00-25*, 62 pp., U.S. Army Corps of Eng., Washington, D. C.

Gabet, E. J. (2003), Sediment transport by dry ravel, *J. Geophys. Res.*, *108*(B1), 2049, doi:10.1029/2001JB001686.

Gabet, E. J., and T. Dunne (2003a), Sediment detachment by rain power, *Water Resour. Res.*, *39*(1), 1002, doi:10.1029/2001WR000656.

Gabet, E. J., and T. Dunne (2003b), A stochastic sediment delivery model for a steep Mediterranean landscape, *Water Resour. Res.*, *39*(9), 1237, doi:10.1029/2003WR002341.

Gilley, J. E., and M. A. Weltz (1995), Hydraulics of overland flow, in *USDA-Water Erosion Prediction Project*, *Rep. 10*, pp. 10.1–10.7, Natl. Soil Erosion Res. Lab., West Lafayette, Ind.

Govers, G., and G. Rauws (1986), Transporting capacity of overland flow, on plane and on irregular beds, *Earth Surf. Processes Landforms*, *11*, 515–524.

Gray, D. H., and W. F. Megahan (1981), Forest vegetation removal and slope stability in the Idaho Batholith, *USDA For. Serv. Res. Pap. INT-271*, 23 pp., Intermt. For. and Range. Exper. Stn., Ogden, Utah.

Gregory, K. J. (1976), Drainage networks and climate, in *Geomorphology and Climate*, edited by E. Derbyshire, pp. 289–315, Wiley-Interscience, Hoboken, N. J.

Gregory, K. J., and V. Gardiner (1975), Drainage density and climate, *Z. Geomorph. N. F.*, *19*, 287–298.

Hack, J. T., and J. C. Goodlett (1960), Geomorphology and forest ecology of a mountain region in the Central Appalachians, *U.S. Geol. Surv. Prof. Pap.*, *347*, 66 pp.

Hanks, T. C. (2000), The age of scarplike landforms from diffusion-equation analysis, in *Quaternary Geochronology: Methods and Applications*, *AGU Ref. Shelf Ser.*, vol. 4, edited by J. S. Noller et al., pp. 313–338, AGU, Washington, D. C.

Hawk, K. L. (1992), Climatology of station storm rainfall in the continental United States: Parameters of the Bartlett-Lewis and Poisson rectangular pulse models, M.S. thesis, 330 pp., Dep. of Civ. and Environ. Eng., Mass. Inst. of Technol., Cambridge.

Horton, R. E. (1945), Erosional development of streams and their drainage basins: Hydrophysical approach to quantitative morphology, *Geol. Soc. Am. Bull.*, *56*, 275–370.

Howard, A. D. (1980), Thresholds in river regimes, in *Thresholds in Geomorphology*, edited by D. R. Coates and J. D. Vitek, pp. 227–258, Allen and Unwin, St Leonards, NSW, Australia.

Howard, A. D. (1994), A detachment-limited model of drainage basin evolution, *Water Resour. Res.*, *30*, 2261–2285.

Howard, A. D. (1997), Badland morphology and evolution: Interpretation using a simulation model, *Earth Surf. Processes Landforms*, *22*, 211–227.

Howard, A. D., and G. Kerby (1983), Channel changes in badlands, *Geol. Soc. Am. Bull.*, *94*, 739–752.

Howes, D. A., and A. D. Abrahams (2003), Modeling runoff in a desert shrubland ecosystem, Jornada Basin, New Mexico, *Geomorphology*, *53*, 45–73.

Istanbulluoglu, E., D. G. Tarboton, R. T. Pack, and C. Luce (2002), A probabilistic approach for channel initiation, *Water Resour. Res.*, *38*(12), 1325, doi:10.1029/2001WR000782.

Istanbulluoglu, E., D. G. Tarboton, R. T. Pack, and C. Luce (2003), A sediment transport model for incision of gullies on steep topography, *Water Resour. Res.*, *39*(4), 1103, doi:10.1029/2002WR001467.

Istanbulluoglu, E., D. G. Tarboton, R. T. Pack, and C. Luce (2004), Modeling of the interactions between forest vegetation, disturbances and sediment yields, *J. Geophys. Res.*, *109*, F01009, doi:10.1029/2003JF000041.

Jahn, A. (1981), Some regularities of soil movement on the slope as exemplified by the observations in Sudety Mts., *Trans. Jpn. Geomorphol. Union*, *2*, 321–328.

Jahn, A. (1989), The soil creep of slopes in different altitudinal and ecological zones of Sudeten Mountains, *Geogr. Ann.*, *71A*, 161–170.

Karsian, E. A. (1995), A 6800-year vegetation and fire history in the Bitterroot Range, Montana, M.S. thesis, Univ. of Montana, Bozeman.

Kelsey, H. M., and J. G. Bockheim (1994), Costal landscape evolution as a function of eustasy and surface uplift rates, Cascadia margin, southern Oregon, *Geol. Soc. Am. Bull.*, *106*, 840–854.

Kirchner, J. W., R. C. Finkel, C. S. Riebe, D. E. Granger, J. L. Clayton, J. G. King, and W. F. Megahan (2001), Mountain erosion over 10 yr, 10 k.y., and 10 m.y. time scales, *Geology*, *29*, 591–594.

Kirkby, M. J. (1971), Hillslope process-response models based on the continuity equation, *Inst. Brit. Geogr. Spec. Publ.*, *3*, 15–30.

Kirkby, M. J., and R. J. Chorley (1967), Throughflow, overland flow and erosion, *Bull. Int. Assoc. Sci. Hydrol.*, *12*, 5–21.

Kobor, J. S., and J. J. Roering (2004), Systematic variation of bedrock channel gradients in the central Oregon Coast Range: Implications for rock uplift and shallow landsliding, *Geomorphology*, *62*, 239–256.

Laflen, J. M., W. J. Elliot, R. Simanton, S. Holzhey, and K. D. Kohl (1991), WEPP soil erodibility experiments for rangeland and cropland soils, *J. Soil Water Conserv.*, *46*, 39–44.

Laio, F., A. Porporato, C. P. Fernandez-Illescas, and I. Rodriguez-Iturbe (2001), Plants in water-controlled ecosystems: Active role in hydrologic processes and response to water stress. IV. Discussion of real cases, *Adv. Water Res.*, *24*, 745–762.

Lancaster, S. T., S. K. Hayes, and G. E. Grant (2003), Effects of wood and debris flow runout in small mountain watersheds, *Water Resour. Res.*, *39*(6), 1168, doi:10.1029/2001WR001227.

Langbein, W. B., and S. A. Schumm (1958), Yield of sediment in relation to mean annual precipitation, *Eos Trans AGU*, *39*, 1076–1084.

Laursen, E. M. (1958), The total sediment load of streams, *Proc. Am. Soc. Civ. Eng. J. Hydraul. Div.*, *84*, 1–6.

Levins, R. (1969), Some demographic and genetic consequences of environmental heterogeneity for biological control, *Bull. Entomological Soc. Am.*, *15*, 237–240.

Long, C. J. (1995), Fire history of the Central Oregon Coast Range, Oregon: 9000-year record from Little Lake, M.S. thesis, 147 pp., Univ. of Oreg., Eugene.

Malmon, D., and T. Dunne (1996), Sediment transport rates by rainsplash based on field measurements, *Eos Trans. AGU*, *77*(46), Fall Meet. Suppl., F254.

May, C. L. (2002), Debris flows through different forest age classes in the Central Oregon Coast Range, *J. Am. Water Resour. Assoc.*, *38*, 1097–1113.

McKean, J. A., W. E. Dietrich, R. C. Finkel, J. R. Southon, and M. W. Caffee (1993), Quantification of soil production and downslope creep rates from cosmogenic 10-Be accumulations on a hillslope profile, *Geology*, *21*, 343–346.

Megahan, W. F., N. F. Day, and T. M. Bliss (1978), Landslide occurrence in the western and central northern rocky mountain physiographic province in Idaho, in *Fifth North American Forest Soils Conference*, edited by C. T. Youngberg, pp. 116–139, Colo. State Univ., Fort Collins.

Melton, M. A. (1957), An analysis of the relations among elements of climate, surface properties and geomorphology, *Dept. Geol. Columbia Univ. Tech. Rep. 11*, *Proj. NR 389-042*, Off. of Nav. Res., New York.

Meyer, G. A., and S. G. Wells (1997), Fire-related sedimentation events on alluvial fans, Yellowstone National Park, USA, *J. Sediment. Res.*, *67*, 776–791.

Meyer, G. A., J. L. Pierce, S. H. Wood, and A. J. T. Jull (2001), Fire, storms and erosional events in the Idaho Batholith, *Hydrol. Processes*, *15*, 3025–3038.

Mitas, L., and H. Mitasova (1998), Distributed soil erosion simulation for erosion prevention, *Water Resour. Res.*, *34*, 505–516.

Moglen, G. E., and R. L. Bras (1995), The effects of spatial heterogeneities on geomorphic expression in a model of basin evolution, *Water Resour. Res.*, *31*, 2613–2623.

Moglen, G. E., E. A. B. Eltahir, and R. L. Bras (1998), On the sensitivity of drainage density to climate change, *Water Resour. Res.*, *34*, 855–862.

Montgomery, D. R. (2001), Slope distributions, threshold hillslopes, and steady-state topography, *Am. J. Sci.*, *301*, 432–454.

Montgomery, D. R., and W. E. Dietrich (1988), Where do channels begin, *Nature*, *336*, 232–234.

Montgomery, D. R., and W. E. Dietrich (1989), Source areas, drainage density and channel initiation, *Water Resour. Res.*, *25*, 1907–1918.

Montgomery, D. R., and W. E. Dietrich (1994), Landscape dissection and drainage area-slope thresholds, in *Process Models and Theoretical Geomorphology*, edited by M. J. Kirkby, pp. 221–246, John Wiley, Hoboken, N. J.

Moore, I. D., G. J. Burch, and P. J. Wallbrink (1986), Preferential flow and hydraulic conductivity of forest soils, *Soil Sci. Am. J.*, *50*, 876–881.

Moss, A. J. (1989), Impact of droplets and the protection of soils by plant covers, *Aust. J. Soil. Res.*, *27*, 1–16.

Nash, D. B. (1980), Forms of bluffs degraded for different lengths of time in Emmett County, Michigan, USA, *Earth Surf. Processes Landforms*, *5*, 331–345.

Nearing, M. A., L. D. Norton, D. A. Bulgakov, G. A. Larinov, L. T. West, and K. M. Dontsova (1997), Hydraulics and erosion in eroding rills, *Water Resour. Res.*, *33*, 865–876.

Nearing, M. A., J. R. Simanton, L. D. Norton, S. J. Bulygin, and J. Stone (1999), Soil erosion by surface water flow on a stony, semiarid hillslope, *Earth Surf. Processes Landforms*, *24*, 677–686.

Nepf, H. (1999), Drag, turbulence and diffusivity in flow through emergent vegetation, *Water Resour. Res.*, *35*, 479–489.

Nepf, H., and E. Vivoni (2000), Flow structure in depth-limited, vegetated flow, *J. Geophys. Res.*, *105*, 28,547–28,557.

Nielson, D. R., J. W. Biggar, and K. T. Erh (1973), Spatial variability of field-measured soil-water properties, *Hilgardia*, *42*, 215–260.

Personius, S. F. (1995), Late Quaternary stream incision and uplift in the forearc of the Cascadia subduction zone, western Oregon, *J. Geophys. Res.*, *100*, 20,193–20,210.

Pickup, G., and V. H. Chewings (1996), Correlations between DEM-derived topographic indices and remotely-sensed vegetation cover in rangelands, *Earth Surf. Processes Landforms*, *21*, 517–529.

Porporato, A., F. Laio, L. Ridolfi, and I. Rodriguez-Iturbe (2001), Plants in water controlled ecosystems: Active role in hydrologic processes and response to water stress III. Vegetation water stress, *Adv. Water Resour.*, *24*, 725–744.

Porporato, A., F. Laio, L. Ridolfi, K. K. Caylor, and I. Rodriguez-Iturbe (2003), Soil moisture and plant stress dynamics along the Kalahari precipitation gradient, *J. Geophys. Res.*, *108*(D3), 4127, doi:10.1029/2002JD002448.

Prosser, I. P. (1996), Thresholds for channel initiation in historical and Holocene times, Southeastern Australia, in *Advances in Hillslope Pro-*

cesses, edited by M. G. Anderson and S. M. Brooks, pp. 687–708, John Wiley, Hoboken, N. J.
Prosser, I. P., and W. E. Dietrich (1995), Field experiments on erosion by overland flow and their implication for a digital terrain model of channel initiation, *Water Resour. Res.*, *31*, 2867–2876.
Prosser, I. P., and C. J. Slade (1994), Gully formation and the role of valley-floor vegetation, southern Australia, *Geology*, *22*, 1127–1130.
Prosser, I. P., and M. Soufi (1998), Controls on gully formation following forest clearing in a humid temperature environment, *Water Resour. Res.*, *34*, 3661–3671.
Prosser, I. P., W. E. Dietrich, and J. Stevenson (1995), Flow resistance and sediment transport by concentrated overland flow in a grassland valley, *Geomorphology*, *13*, 71–86.
Puigdefábregas, J., and G. Sánchez (1996), Geomorphological implications of vegetation patchiness on semi-arid slopes, in *Advances in Hillslope Processes*, edited by M. G. Anderson, and S. M. Brooks, pp. 1027–1060, John Wiley, Hoboken, N. J.
Rauws, G. (1988), Laboratory experiments on resistance to overland flow due to composite roughness, *J. Hydrol.*, *103*, 37–52.
Ree, W. O., F. L. Wimberley, and F. R. Crow (1977), Manning's n and the overland flow equation, *Trans. ASAE*, *20*, 89–95.
Reneau, S. L., and W. E. Dietrich (1991), Erosion rates in the Southern Oregon Coast Range: Evidence for an equilibrium between hillslope erosion and sediment yields, *Earth Surf. Processes Landforms*, *16*, 307–322.
Roering, J. J., J. W. Kirchner, and W. E. Dietrich (1999), Evidence for nonlinear diffusive sediment transport on hillslopes and implications for landscape morphology, *Water Resour. Res.*, *35*, 853–887.
Roering, J. J., J. W. Kirchner, L. S. Sklar, and W. E. Dietrich (2001), Hillslope evolution by nonlinear creep and landsliding: An experimental study, *Geology*, *29*, 143–146.
Roering, J. J., P. Almond, P. Tonkin, and J. McKean (2002), Soil transport driven by biological processes over millenial timescales, *Geology*, *30*, 1115–1118.
Roering, J. J., K. M. Schmidt, J. D. Stock, W. E. Dietrich, and D. R. Montgomery (2003), Shallow landsliding, root reinforcement, and the spatial distribution of trees in the Oregon Cost Range, *Can. Geotech. J.*, *40*, 237–253.
Schmidt, K. M., J. J. Roering, J. D. Stock, W. E. Dietrich, and D. R. Montgomery (2001), The variability of root cohesion as an influence on shallow landslide susceptibility in the Oregon Coast Range, *Can. Geotech. J.*, *38*, 995–1024.
Selby, M. J. (1974), Rates of creep in pumiceous soils and deposits, central North Island, New Zealand, *N. Z. J. Sci.*, *17*, 47–48.
Selby, M. J. (1993), *Hillslope Materials and Processes*, 451 pp., Oxford Univ. Press, New York.
Sidle, R. C. (1992), A theoretical model of the effects of timber harvesting on slope stability, *Water Resour. Res.*, *28*, 1897–1910.
Sklar, L., and W. E. Dietrich (1998), River longitudinal profiles and bedrock incision models: Stream power and the influence of sediment supply, in *Rivers Over Rock: Fluvial Processes in Bedrock Channels*, *Geophys. Monogr. Ser.*, vol. 107, edited by K. J. Tinkler and E. E. Wohl, pp. 237–260, AGU, Washington, D. C.
Sklar, L., and W. E. Dietrich (2004), A mechanistic model for river incision into bedrock by saltating bed load, *Water Resour. Res.*, *40*, W06301, doi:10.1029/2003WR002496.
Smith, T. R., and F. P. Bretherton (1972), Stability and the conservation of mass in drainage basin evolution, *Water Resour. Res.*, *8*, 1506–1529.
Stock, J. D., and W. E. Dietrich (2003), Valley incision by debris flows: Evidence of a topographic signature, *Water Resour. Res.*, *39*(4), 1089, doi:10.1029/2001WR001057.
Tarboton, D. G., R. L. Bras, and I. Rodriguez-Iturbe (1992), A physical basis for drainage density, *Geomorphology*, *5*, 59–76.
Tilman, D. (1994), Competition and biodiversity in spatially structured habitats, *Ecology*, *75*, 2–16.
Tucker, G. E. (2004), Drainage basin sensitivity to tectonic and climatic forcing: Implications of a stochastic model for the role of entrainment and erosion thresholds, *Earth Surf. Processes Landforms*, *29*, 185–205.
Tucker, G. E., and R. L. Bras (1998), Hillslope processes, drainage density and landscape morphology, *Water Resour. Res.*, *34*, 2751–2764.
Tucker, G. E., and R. L. Bras (2000), A stochastic approach to modeling drainage basin evolution, *Water Resour. Res.*, *36*, 1953–1964.
Tucker, G. E., and R. Slingerland (1997), Drainage basin responses to climate change, *Water Resour. Res.*, *33*, 2031–2047.
Tucker, G. E., and K. X. Whipple (2002), Topographic outcomes predicted by stream erosion models: Sensitivity analysis and intermodel comparison, *J. Geophys. Res.*, *107*(B9), 2179, doi:10.1029/2001JB000162.
Tucker, G. E., F. Caini, A. Rinaldo, and R. L. Bras (2001a), Statistical analysis of drainage density from digital terrain data, *Geomorphology*, *36*, 187–202.
Tucker, G. E., S. T. Lancaster, N. M. Gasparini, and R. L. Bras (2001b), The channel-hillslope integrated landscape development model, in *Landscape Erosion and Evolution Modeling*, edited by R. S. Harmon and W. W. Doe, pp. 349–384, Springer, New York.
Tucker, G. E., S. T. Lancaster, N. M. Gasparini, and R. L. Bras (2001c), An object-oriented framework for hydrologic and geomorphic modeling, *Comput. Geosci.*, *27*, 12,229–12,243.
van Wijk, M. T., and I. Rodriguez-Iturbe (2002), Tree-grass competition in space and time: Insights from a simple cellular automata model based on ecohydrological dynamics, *Water Resour. Res.*, *38*(9), 1179, doi:10.1029/2001WR000768.
Wells, W. G. (1987), The effects of fire on the generation of debris flows in southern California, *Rev. Eng. Geol.*, *7*, 105–114.
Whipple, K. X. (2001), Fluvial landscape response time: How plausible is steady-state denudation, *Am. J. Sci.*, *301*, 313–325.
Whipple, K. X., and G. E. Tucker (2002), Implications of sediment-flux-dependent river incision models for landscape evolution, *J. Geophys. Res.*, *107*(B2), 2039, doi:10.1029/2000JB000044.
Willgoose, G., R. L. Bras, and I. Rodriguez-Iturbe (1991), A coupled channel network growth and hillslope evolution model: 1. Theory, *Water Resour. Res.*, *27*, 1671–1684.
Wilson, L. (1973), Variations in mean annual sediment yield as a function of mean annual precipitation, *Am. J. Sci.*, *273*, 335–349.
Woolhiser, D. A., R. E. Smith, and D. C. Goodrich (1990), KINEROS, a kinematic runoff and erosion model: Documentation and user manual, *Rep. ARS-77*, 130 pp., U.S. Dep. of Agric. Agric. Res. Serv., Tuscon, Ariz.
Wu, W., and R. C. Sidle (1995), A distributed slope stability model for steep forested watersheds, *Water Resour. Res.*, *31*, 2097–2110.
Yang, C. T. (1996), Sediment Transport: Theory and Practice, 396 pp., McGraw-Hill, New York.
Young, A. (1972), *Slopes*, Oliver and Boyd, White Plains, New York.

R. L. Bras and E. Istanbulluoglu, Department of Civil and Environmental Engineering, Room 48-114, Massachusetts Institute of Technology, 15 Vassar Street, Cambridge, MA 02139, USA. (rlbras@mit.edu; erkan@mit.edu)